

The Holocene

Linking modern pollen accumulation rates to biomass: Quantitative vegetation reconstruction in the western Klamath Mountains

Journal:	<i>The Holocene</i>
Manuscript ID	HOL-20-0153.R1
Manuscript Type:	Paper
Date Submitted by the Author:	n/a
Complete List of Authors:	Knight, Clarke; UC Berkeley, ESPM Baskaran, Mark; Wayne State University Bunting, M.; University of Hull, Geography Champagne, Marie; USGS Potts, Matthew; UC Berkeley, ESPM Wahl, David; USGS, Wanket, James; California State University Sacramento, Geography Battles, John; UC Berkeley, ESPM
Keywords:	Pollen accumulation rate (PAR), quantitative reconstruction, biomass, source area of pollen, Klamath Mountains, California, pollen
Abstract:	Quantitative reconstructions of vegetation abundance from sediment-derived pollen systems provide insights into past ecological conditions. Recently, the use of pollen accumulation rates (PAR, grains cm ⁻² yr ⁻¹) has shown promise as a bioproxy for plant abundance. However, successfully reconstructing region-specific vegetation dynamics using PAR requires that accurate assessments of pollen deposition processes be quantitatively linked to spatially-explicit measures of plant abundance. Our study addressed these methodological challenges. Modern PAR and vegetation data were obtained from seven lakes in the western Klamath Mountains, California. To determine how to best calibrate our PAR-biomass model, we first calculated the spatial area of vegetation where vegetation composition and patterning is recorded by changes in the pollen signal using two metrics. These metrics were an assemblage-level relevant source area of pollen (aRSAP) derived from extended R-value analysis and a taxon-specific relevant source area of pollen (tRSAP) derived from PAR regression. To the best of our knowledge, aRSAP and tRSAP have not been directly compared. We found that the tRSAP estimated a smaller area for some taxa (e.g., a circular area with a 225 m radius for <i>Pinus</i>) than the aRSAP (a circular area with a 625 m radius). We fit linear models to relate PAR values from modern lake sediments with empirical, distance-weighted estimates of aboveground live biomass (AGLdw) for both the aRSAP and tRSAP distances. In both cases, we found that the PARs of major tree taxa – <i>Pseudotsuga</i> , <i>Pinus</i> , <i>Notholithocarpus</i> , and TCT – were statistically significant and reasonably precise estimators of contemporary AGLdw. However, predictions weighted by the distance defined by aRSAP tended

1
2
3
4
5
6
7
8
9
10
11
12
13
14
15
16
17
18
19
20
21
22
23
24
25
26
27
28
29
30
31
32
33
34
35
36
37
38
39
40
41
42
43
44
45
46
47
48
49
50
51
52
53
54
55
56
57
58
59
60

	to be more precise. The relative root-mean squared error for the aRSAP biomass estimates was 9% compared to 12% for tRSAP. Our results demonstrate that calibrated PAR-biomass relationships provide a robust method to infer changes in past plant biomass.



1
2
3
4
5
6
7
8
9
10 1 Title: Linking modern pollen accumulation rates to biomass: Quantitative vegetation
11 2 reconstruction in the western Klamath Mountains
12
13 3
14
15 4 Authors: Clarke A. Knight¹, Mark Baskaran², M. Jane Bunting³, Marie Champagne⁴, Matthew D.
16 5 Potts¹, David Wahl^{4,5}, James Wanket⁶, John J. Battles¹
17
18 6 ¹ Department of Environmental Science, Policy, and Management, University of California,
19 7 Berkeley, Berkeley, California 94720 USA
20
21 8 ² Department of Geology, Wayne State University, Detroit, Michigan 48202 USA
22
23 9 ³ Department of Geography, Geology and Environment, University of Hull, Cottingham Road,
24 10 Hull, HU6 7RX UK
25
26 11 ⁴ US Geological Survey, Menlo Park, California 94025 USA
27
28 12 ⁵ Department of Geography, University of California, Berkeley, Berkeley, California 94720 USA
29
30 13 ⁶ Department of Geography, California State University, Sacramento, Sacramento, California
31 14 95819 USA
32
33
34 15
35
36 16 Corresponding author: CAK, clarke.knight@berkeley.edu
37
38
39
40
41
42
43
44
45
46
47
48
49
50
51
52
53
54
55
56
57
58
59
60

17 **Abstract**

18 Quantitative reconstructions of vegetation abundance from sediment-derived pollen systems
19 provide unique insights into past ecological conditions. Recently, the use of pollen accumulation
20 rates (PAR, grains cm⁻² yr⁻¹) has shown promise as a bioproxy for plant abundance. However,
21 successfully reconstructing region-specific vegetation dynamics using PAR requires that
22 accurate assessments of pollen deposition processes be ~~deterministically-quantitatively~~ linked to
23 spatially-explicit measures of plant abundance. Our study addressed these methodological
24 challenges. Modern PAR and vegetation data were obtained from seven lakes in the western
25 Klamath Mountains, California. To determine how to best calibrate our PAR-biomass model, we
26 first calculated the spatial area of vegetation where vegetation composition and patterning is
27 recorded by changes in the pollen signal using two metrics. These metrics were an assemblage-
28 level relevant source area of pollen (aRSAP) derived from extended R-value analysis (*sensu*
29 Sugita 1993) and a taxon-specific relevant source area of pollen (tRSAP) derived from PAR
30 regression (*sensu* Jackson 1990). To the best of our knowledge, aRSAP and tRSAP have not
31 been directly compared. We found that the tRSAP estimated a smaller area for some taxa (e.g., a
32 circular area with a 225 m radius for *Pinus*) than the aRSAP (a circular area with a 625 m
33 radius). We fit linear models to relate PAR values from modern lake sediments with empirical,
34 distance-weighted estimates of aboveground live biomass (AGL_{dw}) for both the aRSAP and
35 tRSAP distances. In both cases, we found that the PARs of major tree taxa – *Pseudotsuga*, *Pinus*,
36 *Notholithocarpus*, and TCT (Taxodiaceae, Cupressaceae, and Taxaceae families) – were
37 statistically significant and ~~reliable-reasonably precise~~ estimators of contemporary AGL_{dw}.
38 However, predictions weighted by the distance defined by aRSAP tended to be more precise.
39 The relative root-mean squared error for the aRSAP biomass estimates was 9% compared to 12%

1
2
3
4
5
6
7
8
9
10 40 for tRSAP. Our results demonstrate that calibrated PAR-biomass relationships provide a robust
11 41 method to infer changes in past plant biomass.
12
13 42

14
15 43 **Key words:**

16 44 Pollen accumulation rate (PAR), quantitative reconstruction, biomass, source area of pollen,
17
18 45 Klamath Mountains, California
19
20
21
22
23
24
25
26
27
28
29
30
31
32
33
34
35
36
37
38
39
40
41
42
43
44
45

46 1. Introduction

47 Quantitative reconstruction of past plant abundance has been an important goal in paleoecology
48 since the field's inception (Von Post 1918) and a major research frontier spanning decades
49 (Davis and Deevey 1964, Likens and Davis 1975, Davis et al. 1984, Hicks 2001, Seppä et al.
50 2009, Matthias and Giesecke 2014, Marquer et al. 2014). ~~Currently, t~~The research community
51 lacks a complete understanding of how the pollen signal reflects plant population parameters
52 (e.g., biomass), and therefore past population change (Fagerlind 1952, Davis et al. 1984, Prentice
53 1988, Seppä et al. 2009). Developing methods to quantitatively reconstruct past plant
54 populations would aid climate science and restoration ecology. In climate science, for example,
55 quantitative reconstructions of past plant populations would allow better understanding of long-
56 term ecosystem dynamics (Galliard et al. 2000) and provide past analogues to test complex
57 climate models that account for the effects of landcover on the climate system (Galliard et al.
58 2010). Restoration ecology would benefit from an improved understanding of the impact of
59 disturbances (natural and anthropogenic) on landscapes and ecosystems (Broström et al. 1998,
60 Crawford et al. 2015) and from the increased participation by paleo-ecologists in the debates of
61 modern restoration ecology (Swetnam et al. 1999, Hellman et al. 2009).

62 Palynologists often use pollen percentage data in pollen-vegetation models to reconstruct
63 landcover and understand past plant populations, but this approach does not provide separate
64 reconstructions for each taxon's ~~plant~~ population change (Davis 1963, Prentice 1988). Relative
65 changes in abundance of species have been inferred from Bayesian hierarchical spatio-temporal
66 pollen-vegetation models (Dawson et al. 2019). In contrast, pollen accumulation rates (PAR) – a
67 measure of the rate of pollen deposition at the sediment surface per unit area during a given time
68 period (e.g., grains cm⁻² yr⁻¹, Davis and Deevey 1964) – depend ~~solely~~ on the abundance of the

Commented [MOU1]: Added sentence for USGS reviewer.

1
2
3
4
5
6
7
8
9
10 69 plant taxa producing that pollen type around the collection site. That is, the PAR for each taxon
11 70 is independent of all other taxa. PAR allows results from different regions to be directly
12
13 71 compared, irrespective of other taxa in the investigations ([Hicks and Hyvärinen 1999](#), [Giesecke](#)
14 72 [and Fontana 2008](#)). PAR has been used to reconstruct not only landcover, but also population
15
16 73 dynamics and plant biomass (Seppä et al. 2009, Theuerkauf et al. 2012, Matthias and Giesecke
17
18 74 2014). For example, PAR has been used to reconstruct past population growth rates (Bennett
19
20 75 1983, 1986, MacDonald 1993, Giesecke 2005) and to reconstruct Holocene biomass records in at
21
22 76 least two areas: the Finnish boreal zone (Seppä et al. 2009) and a sub-alpine forest in Utah
23
24 77 (Morris et al. 2015).

25 78 PAR is not a simple reflection of vegetation abundance because the pollen signal is a
26
27 79 distance-weighted measure of taxa abundance in the surrounding vegetation, responding to the
28
29 80 structure of the plant community as well as species abundance (Jackson 1990). Modern PAR
30
31 81 values must be quantitatively correlated with modern plant population data from the lake
32
33 82 surroundings in order to parameterize the PAR-population relationship before fossil PAR records
34
35 83 can be interpreted in terms of past plant population change. This correlation step requires
36
37 84 accurate vegetation data from forest inventories (Seppä et al. 2009, Matthias and Giesecke 2014),
38
39 85 careful field surveys (Bunting et al. 2013), or well-resolved spatial imagery coupled with
40
41 86 ground-truthing (Han et al. 2017) that encompasses the relevant source area of pollen ('RSAP',
42
43 87 discussed below and in section 2.3, *sensu* Sugita 1993). Previous work has shown a linear
44
45 88 relationship between PAR and distance-weighted biomass across a range of lake sites in
46
47 89 northeastern Germany (Matthias and Giesecke 2014).

48 90 In addition to quantitative vegetation data, reliable PAR data require a robust chronology
49
50 91 of the pollen system being studied. Ideally, a sedimentary core for PAR data collection has two

1
2
3
4
5
6
7
8
9
10 92 features: it is obtained from an undisturbed lake environment where sediment accumulates
11 93 evenly over time, and the resulting sediment is dated at high resolution. Where lakes are found to
12 94 have stable sedimentary conditions, reliable PAR datasets can be obtained (e.g., Ritchie 1969,
13 95 Hyvärinen 1975, Seppä and Hicks 2006) though there may still be channel funneling. The recent
14 96 development of Bayesian tools has improved the construction of chronologies from isotopic data
15 97 such as ^{210}Pb activity measurements, giving more reliable measures of uncertainty (Aquino-
16 98 López et al. 2018).

17
18
19
20
21
22 99 Lastly, all sedimentary basins have a relevant source area of pollen (RSAP), which is
23 100 sometimes referred to as the “pollenshed” of the basin (*sensu* Sugita 1993). The basic premise is
24 101 that vegetation within a certain area-distance of the basin corresponds to the quantity and type of
25 102 pollen deposited at the site. With distance from the lake shore, ~~C~~correlations between plant
26 103 abundance and pollen loading are expected to improve ~~close to the lake shore~~, then approach an
27 104 asymptote at some distance because source vegetation of pollen far from the basin should have
28 105 much less influence on the pollen representation than vegetation closer to the basin. Estimating
29 106 the RSAP is a key step for quantitative calibration because it provides information about the
30 107 spatial extent of any subsequent vegetation reconstruction (Sugita et al. 1999, Bunting et al.
31 108 2004, Hellman et al. 2009). To our knowledge, the distinction between an assemblage-level
32 109 pollenshed RSAP (aRRSAP, Sugita 1993) and taxa-specific RSAPpollensheds (tRRSAP, *sensu*
33 110 Jackson 1990, Matthias and Giesecke 2014) has not yet been drawn within the same basin (Table
34 111 X). Comparing these estimates provides insight about how pollen assemblages “sense”
35 112 vegetation, which is critical to the extraction of vegetation information from pollen data.

36
37
38
39
40
41
42
43
44
45
46 113 Given the methodological challenges, the application of calibrated PAR-biomass transfer
47 114 functions to any ecosystem is not routine. This paper develops PAR-biomass models using short
48
49
50
51
52
53
54
55
56
57
58
59
60

1
2
3
4
5
6
7
8
9
10 115 cores from seven small lakes in the western Klamath Mountains, California, and follows the
11 116 general approach used in previous studies (e.g., Seppä et al. 2009, Matthias and Giesecke 2014)
12
13 117 whilst critically evaluating each step in the process. The Klamath bioregion contains numerous
14
15 118 small lakes and is an area where Holocene-length paleoecological records have already provided
16
17 119 a portrait of ecological change (Fig. 1). We measured modern PAR from lake sediments and
18
19 120 acquired vegetation abundance data to achieve three goals: 1) to understand the spatial
20 121 relationship between pollen assemblages-flux in small lakes and surrounding vegetation cover,
21
22 122 through modeling of the aRSAP and tRSAP, 2) to calibrate a PAR-biomass model using
23
24 123 distance-weighted biomass for major tree taxa, and 3) to assess the potential of this model to
25 124 reconstruct past changes in assemblage-wide biomass from the region.
26
27 125
28

29 126 **2. Background**

30 127 Below, we describe the study area's physical features (2.1), our pollen-vegetation modelling
31
32 128 approach (2.2), and the methodology used to estimate aRSAP and tRSAP (2.3).
33
34 129

36 130 *2.1 Study Area*

37 131 The Klamath bioregion, a physically and floristically diverse area in northwestern California
38
39 132 (Whittaker 1960, Cheng 2004), contains hundreds of small lakes. Many lakes are found at high
40
41 133 elevations and are glacial in origin, but there are also landslide-created lakes at low- and mid-
42
43 134 elevations in the western portion of the region (Wahrhaftig and Birman 1965). The landscape has
44
45 135 deep catchments and steep mountains (Irwin 1981), and the climate is Mediterranean, consisting
46 136 of cool, wet winters and warm, dry summers (Skinner et al. 2006). Prior to 20th century fire
47
48
49
50
51
52
53
54
55
56
57
58
59
60

1
2
3
4
5
6
7
8
9
10
11
12
13
14
15
16
17
18
19
20
21
22
23
24
25
26
27
28
29
30
31
32
33
34
35
36
37
38
39
40
41
42
43
44
45
46
47
48
49
50
51
52
53
54
55
56
57
58
59
60

137 suppression, the landscape had a mixed-severity fire regime characterized by mostly small, low-
138 intensity, frequent fires, and infrequent large burns of mixed-severity (Taylor and Skinner 2003).

139 Our study focused on the western Klamath Mountains where low-elevation forests
140 (<600–800 m) are dominated by *Pseudotsuga menziesii* (Douglas-fir). Multiple *Pinus* (pine)
141 species including *Pinus lambertiana* (sugar pine), *Pinus jeffreyi* (Jeffrey pine), and *Pinus*
142 *ponderosa* (ponderosa pine) are also common but less frequent than Douglas-fir. The most
143 common broadleaf tree species in the low-elevation forests are *Notholithocarpus densiflorus*
144 (tanoak), followed by *Arbutus menziesii* (Pacific madrone), *Chrysolepis chrysophylla* (golden
145 chinquapin), and *Quercus kelloggii* (California black oak). *Chamaecyparis lawsoniana* (Port-
146 Orford-cedar) is mainly found in riparian areas but can be found on slopes. Higher-elevation
147 montane forests are dominated by *Abies concolor* (white fir) and *Abies magnifica* (red fir;
148 Sawyer and Thornburg, 1977), whereas sub-alpine (above ~1700 m) zones include *Tsuga*
149 *mertensiana* (mountain hemlock) and *Picea breweriana* (Brewer spruce) (Sawyer and Thornburg
150 1977). On areas of ultramafic soils derived from serpentinite and peridotite bedrock, Jeffrey pine,
151 *Pinus monticola* (western white pine) and *Calocedrus decurrens* (incense-cedar) are the
152 dominant forest taxa (Whittaker 1960; nomenclature follows Hickman 1993).

153 We selected seven small lakes in the Six Rivers National Forest with small basins, and
154 minimal stream inputs, and shallow slopes (Table 1, Fig. 1). Vegetation around the lakes is
155 representative of the diverse mixed conifer forest of the Klamath bioregion (Hudiburg et al.
156 2009) although the dominant overstory varies at each lake site. Holocene-length pollen records
157 (percentage and PAR) already exist for three of the seven lakes and suggest that the modern
158 forest structure and composition have been relatively stable for the last 2,000 years (Wanket

1
2
3
4
5
6
7
8
9
10 159 2002) but also imply a 3,000-year historic high of Douglas-fir in the contemporary forest
11 160 (Crawford et al. 2015).

13 161 2.2 Pollen-vegetation models

14
15 162 Linear pollen-vegetation models (PVMs) have a long history of use in palynology (Davis 1963,
16 163 2000; Andersen 1970; Prentice 1985, 1988; Sugita 1993, 1994; Bunting and Middleton 2005,
17 164 Bunting et al. 2013). PVMs use the relationship between pollen assemblages and vegetation to
18 165 infer past vegetation composition or structure from fossil pollen data. The main strengths of
19 166 linear PVMs are: 1) they provide the means to reconstruct vegetation from landscapes with no
20 167 modern analogue; 2) they have been widely tested against empirical data in quantitative
21 168 reconstruction research (e.g., Davis 1963, Andersen 1970, Prentice 1985, Sugita 1993, Bunting
22 169 and Hjelle 2010); and 3) they have been successfully validated in at least one region (southern
23 170 Sweden, Sugita 2007a, b; Hellman et al. 2008a, b).

30 171 In this work, we used a version of Sutton's original PVM model (Sutton 1947, 1953)
31 172 inverted by Prentice (1985) and modified by Sugita (1994) for lake environments. This model's
32 173 form – called Prentice-Sugita-Sutton – assumes that pollen could land anywhere on the lake
33 174 surface and would be perfectly mixed in the water column before being deposited on the lakebed.
34 175 The Prentice-Sugita-Sutton model also assumes that pollen transport is largely via wind above
35 176 the canopy and gravity beneath the canopy, and that the sampling basin is circular with uniform
36 177 wind in every direction (Sugita 1994, [full list of assumptions in the supplement](#)). Under this
37 178 approach, we a) divide the vegetation into rings, b) distance-weight each ring, and c) compare
38 179 the PAR from the basin with the summed distance weighting from one or more rings, working
39 180 out from the edge of the basin. This model calculates the total pollen influx from each source
40 181 across the whole lake. Its simplest linear form is:

Commented [MOU2]: Addressed Reviewer 3 concern about "hidden assumptions."

$$Y_{ik} = \alpha_i \cdot \psi_{ik} \quad (1)$$

where,

Y_{ik} = pollen influx for a taxon i at site k

α_i = pollen productivity of taxon i

ψ_{ik} = the distance-weighted plant abundance (DWPA) of taxon i around site k with the weighting term reflecting the pollen dispersal of taxon i (weighting term calculation shown in [Equation 3](#)).

DWPA (ψ_{ik}) is defined as:

$$\Psi_{ik} = \int_R^\infty X_{ik}(z)g_i(z)dz \quad (2)$$

where,

R = the radius of the canopy opening in which the sample site is located

$X_{ik}(z)$ = the plant abundance measure consisting of the contribution of taxon i to the pollen assemblage formed at site k from plants located distance z from sampling location k , and $g_i(z)$ is the distance weighting term for taxon i at distance z from any sampling location.

The Prentice-Sugita-Sutton weighting term g_i for taxon i at distance z is calculated using:

$$g_i(z) = b_i \gamma z^{\gamma-1} e^{-b_i z^\gamma} \quad (3)$$

$$\text{where } b_i = \frac{4v_g}{\pi u \sqrt{\pi C_z}} \quad (3a)$$

and,

z = distance

γ = a coefficient of 0.125 (Prentice 1985)

v_g = approximated by v_s (fall speed, m sec⁻¹)

205 C_z = the vertical diffusion coefficient ($m^{1/8}$)

206 n = a dimensionless turbulence parameter equal to 2

207 u = windspeed ($m\ sec^{-1}$), set equal to 3.

208 Note that C_z and n depend on atmospheric stability.

209 Equation 2 can be re-written as a sum with two addends: 1) the unique contribution of the
210 vegetation close to site k where ζ is the pollen source area for site k , and 2) the long-distance
211 pollen transport ('background pollen,' which is uniform beyond ζ), giving:

$$\Psi_{ik} = \int_R^\zeta X_{ik}(z)g_i(z) dz + \int_\zeta^\infty X_{ik}(z)g_i(z) dz \quad (4)$$

213 Which can be written as

$$Y_{ik} = \alpha_i \psi_{ik} + \omega_i \quad (5)$$

$$\text{Where } \psi_{ik} = \int_R^\zeta X_{ik}(z)g_i(z) dz$$

217 2.3 Spatial area represented by the pollen record

218 We estimated the spatial extent of our sites' pollenshedsource area of pollen in two ways
219 (definitions in Table 2). We calculated the standard assemblage-specific metric – the relevant
220 source area of pollen (aRSAP) – which is defined as the area beyond which the correlation
221 between pollen and vegetation does not improve (Sugita 1993). Estimates of aRSAP can be
222 extracted from extended R-value (ERV) analysis using pollen percentage data (Parsons and
223 Prentice 1981). ERV analysis is the process of solving n equations for $2n$ unknowns in order to
224 extract the parameter estimates, where ERV sub-models 1, 2 and 3 are the underlying vegetation-
225 pollen relationship models. The three sub-models define background pollen differently (Sugita
226 1994). Whereas models 1 and 2 use pollen data and vegetation percentages (Parsons and Prentice
227 1981), model 3 uses pollen percentages and plant abundance data in absolute units (e.g., biomass

1
2
3
4
5
6
7
8
9
10
11
12
13
14
15
16
17
18
19
20
21
22
23
24
25
26
27
28
29
30
31
32
33
34
35
36
37
38
39
40
41
42
43
44
45
46
47
48
49
50
51
52
53
54
55
56
57
58
59
60

228 per area) (Sugita 1994). Using the maximum likelihood method, ERV models iteratively fit the
229 relationship between pollen and vegetation percentages (Bunting and Hjelle 2010). Maximum
230 likelihood function scores measure the goodness of fit between pollen percentages and distance-
231 weighted plant abundance. The aRSAP can be estimated from visual inspection of the likelihood
232 function score plotted against distance; it is the point at which scores approach an asymptote
233 (Sugita et al. 1999, Bunting et al. 2005).

234 We then calculated a taxon-specific metric of the relevant source area (tRSAP) to
235 compare to the aRSAP. We call the tRSAP the distance beyond which the correlation between
236 PAR and DWPA summed to that distance does not improve (Jackson 1990). We fit a linear
237 equation (equation 5) for each individual taxon because both y and ψ are measured in
238 independent terms. We again used the ring source model, which converts the integral into a
239 summation. That is, we summed the value for each of the rings and $g_i(z)$ includes ring area in
240 this formulation. As with aRSAP, tRSAP can be estimated from visual inspection of the R^2 value
241 against the distance from the lake shore (m) (Matthias and Giesecke 2014).

243 3. Methods

244 Fitting PAR-biomass relationships requires a number of steps shown in a flowchart (Fig. 2) with
245 numbers matching the following sections.

247 3.1 Lake selection and core sampling

248 We used the following criteria to determine suitable lake sites: small size (radius approximately
249 100 m), no permanent outflow, simple basin, and core length greater than 25cm. Ten such lakes
250 were identified from topographical maps and satellite imagery as promising, but each were

1
2
3
4
5
6
7
8
9
10 251 assessed in the field. Out of this collection, seven lakes were viable and selected for ^{210}Pb dating.
11 252 During the summer of 2018, short cores (~50 cm) of 7 cm diameter were taken from each lake's
12 253 center using either a gravity corer (Ogaromtoc, Fish Lakes) or a piston corer (all other lakes).

14 254 The sediment-water interface was immobilized by sodium polyacrylate for transport. Cores were
15 255 later split and sectioned in the laboratory.

18 256 3.2 Sediment dating, age-depth model, and sediment lithology

20 257 We used lead-210 (^{210}Pb ; 22.3 yr half-life) to assign ages to sediment deposited in the last 150
21 258 years. Surface bulk sediments from 0 cm to a maximum of 45 cm were taken from each core and
22 259 dried to 105°C (see Tables S1-S7). ^{210}Pb activity was determined by alpha spectrometry ([see SI](#)
23 260 [for complete dating methodology](#)), via ^{210}Po . An aliquot of 0.2 to 1.0 g of dried and pulverized
24 261 sample was digested using concentrated HF, HNO₃, and HCl and a known amount of ^{209}Po spike
25 262 in an oven at 90°C for ~24 hours. The digested solution was dried, and the residue was mixed
26 263 with 1 M HCl until the pH was ~2. Auto-plating of Po was cold-plated onto an Ag disk for 24
27 264 hours at room temperature (Jweda and Baskaran 2011). The plated disk was assayed for Po using
28 265 Octete PC ORTEC alpha spectrometer. The reagent blanks were run simultaneously with each
29 266 batch of eight samples and were subtracted. Certified reference materials were periodically run.
30 267 For the determination of parent-supported (i.e., background) ^{210}Pb , several samples were run for
31 268 the activity of ^{226}Ra (using 352 and 609 keV) along with ^{137}Cs (661.6 keV) by Ge-well detector
32 269 (Baskaran et al. 2015). Small sample sizes prevented reliable ^{137}Cs from being obtained.

33 270 We used the Bayesian-based Plum software to develop age models from excess (unsupported)
34 271 ^{210}Pb data (Aquino-López et al. 2018). The Plum model is related to the constant rate of supply
35 272 (CRS) method (Appleby and Oldfield 1978) and retains two of the basic assumptions of CRS:
36 273 the rate of supply of ^{210}Pb is constant and there is no vertical mixing of radionuclides. Testing
37
38
39
40
41
42

1
2
3
4
5
6
7
8
9
10
11
12
13
14
15
16
17
18
19
20
21
22
23
24
25
26
27
28
29
30
31
32
33
34
35
36
37
38
39
40
41
42
43
44
45
46
47
48
49
50
51
52
53
54
55
56
57
58
59
60

~~these assumptions requires independent validation using another marker, which is outside of this paper's scope. The Plum model is formulated within a robust statistical framework to quantify uncertainty (Aquino-López et al. 2018). Plum uses a self-adjusting Markov Chain Monte Carlo (MCMC) algorithm called the t-walk (Christen and Fox 2010). Plum uses millions of MCMC iterations to model the accumulation of sediment, using a gamma autoregressive semiparametric age-depth function (Blaauw and Christen 2011). This algorithm results in a probability envelope around the mean age model. The envelope allows the precision at any depth to be estimated explicitly. Plum makes use of prior information to determine the datable horizon, which is affected by two factors: the precision of methodology (alpha versus gamma counting) and the initial amount of excess lead. In Plum, the chronology limit is determined by the rate of supply of ^{210}Pb to the site and the equipment error, usually ~ 3 Bq/kg for a sample size of 1 g by alpha spectrometry for research laboratories. Supported ^{210}Pb activities were determined from the direct measurements of ^{226}Ra by gamma-ray spectrometry.~~

3.3 Pollen analysis

~~Pollen samples one from each lake site were extracted from 0.63 cm³ of wet sediment from the top 0.5 cm of each core and were processed according to standard pollen preparation procedures (Faegri and Iversen 1989) but modified to include two steps: 1) sieving with 5- and 153-micron mesh under vacuum and 2) swirling, with the less dense fractions retained. These steps draw on current US Geological Survey protocol (Tom Sheehan, personal communication), which is based on Doher's palynomorph methodology and current United States Geological Survey procedures (Doher 1980). One *Lycopodium* spore tracer tablets containing 20,848 spores wereas added to each sample to calculate pollen concentration (Stockmarr 1971, Faegri and~~

Commented [MOU3]: Clause added for USGS reviewer

1
2
3
4
5
6
7
8
9
10 297 Iversen 1989). Acetolysis and sieving steps were repeated for samples containing high amounts
11 298 of organic material. Pollen samples were mounted in silicone oil and examined at 500×
12
13 299 magnification. At least 400 terrestrial grains per sample were counted and identified using the
14
15 300 UC Berkeley Museum of Paleontology modern pollen reference collection, as well as pollen
16
17 301 atlases (Knapp 1969, Halbritter et al. 2018).

18 302 Seven wind-pollinated taxa were identified at all sites: *Pinus*, *Pseudotsuga*, *Quercus*,
19
20 303 *Notholithocarpus*, *Alnus*, TCT (Taxodiaceae, Cupressaceae, and Taxaceae families), and *Abies*.
21
22 304 The corresponding plant taxa from the study area were sugar pine, Jeffrey pine, ponderosa pine
23
24 305 (*Pinus*); Douglas-fir (*Pseudotsuga*); California black oak, canyon live oak (*Quercus*); tanoak,
25
26 306 golden chinquapin (*Notholithocarpus*); white alder (*Alnus*); Port-Orford-cedar, incense-cedar
27
28 307 (TCT); white fir, red fir (*Abies*). we only encountered Port-Orford-cedar and incense-cedar in the
29
30 308 vegetation survey at the study sites and assume all TCT originating within the surveyed
31
32 309 vegetation area came from these species. Counts of *Pinus*, *Quercus*, *Notholithocarpus* and *Abies*
33
34 310 reflect all the pollen grains from their respective genera (i.e., we report total *Pinus* which likely
35
36 311 contained sugar pine, Jeffrey pine, and ponderosa pine grains). *Pseudotsuga* and *Alnus* counts
37
38 312 represent the species *Pseudotsuga menziesii* (Douglas-fir) and *Alnus rhombifolia* (white alder).
39
40 313 Other wind-pollinated tree pollen present in trace amounts includes willow (*Salix*), buckthorn
41
42 314 (*Rhamnaceae*), hazel (*Corylus*) and silk tassel (*Garrya*). This group of “other hardwoods”
43
44 315 accounted for only 0.35% of the woody species. Given their rarity, we omitted them from the
45
46 316 determination of pollen source area and subsequent PAR-biomass modeling.

46 318 3.4 PAR determination

47
48 319 Pollen concentrations (grains cm⁻³) and PAR (grains cm⁻² yr⁻¹) were determined using the
49
50
51
52
53
54
55
56
57
58
59
60

320 *Lycopodium* marker grains, pollen concentrations (C_i , grains cm^{-3}) were calculated for each
 321 pollen type i using the following equation:

$$322 \quad C_i = \frac{A_i \times L_e}{L_e \times V_i} \quad (6)$$

323 Where A_i is the number of pollen grains counted for each taxon i , L_e is the number of added
 324 marker grains, L_e is the number of counted marker grains in each slide, and V_i is the volume of
 325 the pollen sample (e.g., 0.63 cm^3) (Stockmarr 1971), and C_i concentrations were used for PAR
 326 calculations by multiplying the concentration values by the sediment accumulation rate (Davis
 327 and Deevey 1964), which differed by lake site and was determined by the Plum age model in
 328 increments of 0.5cm (see SI for equations used). The equation used was:

$$329 \quad PAR_i = C_i \times S \quad (7)$$

330 Where PAR_i is the pollen accumulation rate for taxon i , C_i is the pollen concentration (grains cm^{-3})
 331 for taxon i , and S is the sedimentation rate (cm yr^{-1}) (Davis and Deevey 1964).

333 3.5 Forest inventories

334 We used cruising prisms (wedges of glass with a known size/angle) to determine the basal area
 335 of the dominant pollen-producing taxa within 750 m from each lake's shoreline (USDA Forest
 336 Service 2000). The prism method employs variable plot radius sampling at the stand level.
 337 Transects in eight directions (N, S, E, W, NE, NW, SE, SW) from the lake shore were sampled.
 338 The basal area of live trees was measured using the prisms ~~were taken~~ every 50m along the
 339 transects, following Han et al. 2017 (Fig. 3).

340 We used aboveground live tree biomass (AGL) as the specific measure of abundance that
 341 is distance weighted. To estimate AGL from basal area measurements, we developed species-
 342 specific allometric equations using contemporary data from the US Forest Service Forest

1
2
3
4
5
6
7
8
9
10 343 Inventory and Analysis program (FIA). From the FIA plots inventoried in Six Rivers National
11 344 Forest between 2001 and 2017 (FIADB 2020), we calculated plot-level basal area (m² ha⁻¹) for
12
13 345 every species in the plot and linked it to the estimate of plot-level aboveground live biomass (Mg
14
15 346 ha⁻¹) for each species (n = 3,428 plot-by-species observations). AGL was estimated using the
16
17 347 regional model of tree biomass (Zhou and Hemstrom 2009). For every species, we predicted
18
19 348 AGL as a function of basal area using a linear log-log (natural) equation (*sensu* Knight et al.
20 349 2020).

21
22 350
23
24 351 Specifically,
25 352
$$\ln (AGL_{ij}) = \beta_{0_i} + \beta_{1_i} * \ln (Basal Area_{ij}) \quad (8)$$

26
27 353 where $\ln(AGL_{ij})$ is the natural log of aboveground live biomass for species i in plot j , $\ln(Basal$
28
29 354 $Area_{ij})$ is the natural log of tree basal area for species i in plot j , β_{0_i} is the intercept for species i ,
30
31 355 and β_{1_i} is the slope coefficient for species i . For the six most abundant species that accounted for
32
33 356 90% of the basal area, fits ranged from a low of 0.85 for sugar pine to a high of 0.97 for Port-
34
35 357 Orford-cedar (Table S8). With these equations and field measurements of species basal area, we
36 358 calculated the AGL of each species in the prism sample.

37
38 359

39 360 3.6 ERV analysis and estimation of aRSAP

40
41 361 The aRSAP values were extracted from conventional ERV analysis using model 3. We used
42
43 362 PolERV from the software suite HUMPOL (Bunting and Middleton 2005) which has the same
44
45 363 core code (erv-v6.exe and polsim-v3.exe) as other ERV software, e.g. POLLSCAPE (Sugita
46
47 364 1994). In order to meet the requirement that the number of sites is at least twice the number of
48
49 365 taxa used in ERV analysis (Soepboer et al. 2007), we analyzed sub-sets of three taxa across the

1
2
3
4
5
6
7
8
9
10 366 seven sites using the same reference taxon (TCT) every time. For example, one such sub-set
11 367 combination was TCT, *Pseudotsuga*, and *Pinus*. We selected TCT as the reference taxon (i.e.,
12 368 specified that TCT has a relative pollen productivity of 1.0) for several reasons. First, a scatter
13 369 plot of TCT pollen values and unscaled distance weighted plant abundance is positive and linear
14 370 (Fig. S1). Second, TCT has an estimated relative pollen productivity in the middle of the dataset
15 371 upon ERV analysis with all seven taxa. Lastly, TCT is represented in pollen data at all sites
16 372 (unlike *Abies*, *Alnus*, or *Quercus*), and is present in vegetation close to the [sampling point](#)
17 373 [site](#). aRSAP was estimated by plotting the likelihood scores for each distance across all taxa
18 374 combinations and pooling the results.
19
20
21
22
23
24

375

376 3.7 Distance weighting and estimation of tRSAP

27
28
29 377 AGL results were first averaged by the number of plots in each concentric ring and then each
30 378 ring was weighted using the Prentice-Sugita weighting under stable conditions, [which affect](#)
31 379 [parameters \$C_z\$ and \$n\$](#) (Eq. 3, 3a). We assumed stable atmospheric conditions because simulation
32 380 experiments comparing unstable and stable models demonstrate little difference in estimated
33 381 aRSAP and pollen productivity (Broström et al. 2004). The pollen-specific fall speeds (m sec^{-1})
34 382 of *Abies*, *Alnus*, *Pinus*, *Pseudotsuga*, and *Quercus* have been determined in previous work (Table
35 383 S9). For TCT, Stoke's Law (Gregory 1973) was used to calculate fall speed using the average
36 384 grain size of each taxon and weighted by relative abundance of the contributing species Port-
37 385 Orford-cedar and incense-cedar (both Cupressaceae family). For subprolate grain
38 386 *Notholithocarpus*, major and minor axes were measured from reference slides in UC Berkeley's
39 387 collections, and then Stoke's Law with Falck's (1927) correction was used. Lastly, we
40 388 determined the coefficient of determination (R^2) of the linear model predicted from AGL_{dw} at
41
42
43
44
45
46
47
48
49
50
51

1
2
3
4
5
6
7
8
9
10 389 distance z (AGL_{dwz}) as a function of PAR. The R^2 between PAR and summed AGL_{dw} for each
11 390 ring distance was plotted against the distance. The tRSAP occurs where the line reaches an
12
13 391 asymptote.
14

15 392 16 393 3.8 PAR-biomass transfer equations

18 394 We developed transfer equations to predict taxon-specific contributions to the distance-weighted
19
20 395 AGL (AGL_{dw}) as a function of taxon-specific PAR. Although biomass “predicts” pollen
21
22 396 accumulation rates in a functional sense, our aim was to apply calibrated transfer functions to
23
24 397 predict biomass in the past. Consequently, we fitted regression lines with PAR values as the
25
26 398 independent variable. This reasoning has been used for needle accumulation rate as a predictor of
27
28 399 Holocene-era basal area (Blarquez et al. 2011).

29 400 In this analysis, each lake represented a sample with the depositional source area defined
30
31 401 by either aRSAP or tRSAP. We included seven pollen-producing taxa, namely *Pseudotsuga*,
32
33 402 *Pinus*, *Notholithocarpus*, TCT, *Alnus*, *Quercus*, and *Abies*, that collectively account for greater
34 403 than 99% of the pollen-producing trees present in the surrounding landscape. Using the assigned
35
36 404 source area distances, we calculated AGL_{dw} for the taxa present at each lake and regressed it
37
38 405 against PAR using linear models (see Fig. 8a,b). Specifically, we evaluated three model forms: a
39
40 406 linear model with an intercept term and slope term, a linear model with only a slope term, and
41
42 407 segmented linear model with one breakpoint. In the linear models with intercepts, the intercept
43
44 408 represents the “background” pollen component; because we treated PAR values as the
45
46 409 independent variable, these intercepts are negative. So, we included an origin-forced model as an
47
48 410 option because negative-intercept models are not biologically meaningful for biomass
49
50 411 reconstruction given that very low PAR values would yield negative biomass. We included the

Commented [MOU4]: Added for USGS reviewer.

1
2
3
4
5
6
7
8
9
10
11
12
13
14
15
16
17
18
19
20
21
22
23
24
25
26
27
28
29
30
31
32
33
34
35
36
37
38
39
40
41
42
43
44
45
46
47
48
49
50
51
52
53
54
55
56
57
58
59
60

412 segmented model to potentially capture threshold responses in the relationship between AGL and
413 PAR (Muggeo 2008). We ranked the models by the Akaike Information Criterion for small
414 samples (AICc) in order to compare performance. AICc imposes a stronger penalty on model
415 complexity than AIC and was chosen in order to avoid fitting models which were overly
416 complex given the size of the dataset (Burnham and Anderson 2002).

417 To evaluate the uncertainty introduced by the PAR transfer functions, the AGL_{dw}
418 predicted from PAR at each lake (predicted AGL_{dw}) was compared to the AGL_{dw} calculated from
419 the observed AGL_{dw} . Error was propagated using a resampling method (Crowley et al. 1992).
420 Specifically, we estimated the error in predicted AGL_{dw} for each iteration as a random sample
421 from a normal distribution with the mean equal to zero and the standard deviation equal to the
422 standard error of the regression estimate (SEE) for each taxon. Results were based on 10,000
423 iterations and reported as means and standard errors of the predicted AGL_{dw} for each lake. Bias
424 between the predicted and observed AGL_{dw} was calculated as:

$$Bias = \frac{Predicted\ AGL_{dw} - Observed\ AGL_{dw}}{Observed\ AGL_{dw}} \quad (9)$$

4. Results

4.1 Chronology

429 The seven lakes' chronologies were established using at least 20 ^{210}Pb dates-measurements at
430 each site (see Table S3-S9 for exact number of samples for each core). Blue Lake is shown as an
431 example (Fig. 4). The chronologies for Fish, North Twin, Ogaromtoc, Onion, Red Mountain, and
432 South Twin lakes followed the same procedure (Fig. S2). The lakes are characterized by rapid
433 sedimentation rates, with rates in the upper sediments in the range of 0.14-0.33 $cm\ yr^{-1}$ (3-7 yr
434 cm^{-1}). Therefore, surface samples (upper 0.5cm) contain pollen from 2018 (collection date) to

1
2
3
4
5
6
7
8
9
10 435 2011 at the oldest. Core lithology results are provided in the supplement (Figs. S3-4).

11 436

12
13 437 *4.2 PAR*

14
15 438 A group of highly abundant tree taxa contained *Pseudotsuga*, *Pinus*, *Notholithocarpus*, and TCT,
16
17 439 which were reflected in high ($> 2,000$ grains $\text{cm}^{-2} \text{yr}^{-1}$) PAR values in most samples (Fig. 5,
18
19 440 Table S10). For example, *Pseudotsuga* values were above 5,000 grains $\text{cm}^{-2} \text{yr}^{-1}$ at all sites
20
21 441 except Onion Lake. The highest overall PAR value was *Pinus* at Onion Lake which exceeded
22
23 442 10,000 grains $\text{cm}^{-2} \text{yr}^{-1}$. High PAR values reflect the Douglas-fir and pine-dominant composition
24
25 443 of Six Rivers National Forest. Onion Lake is the only lake situated in the True Fir alliance zone
26
27 444 and, unsurprisingly, the *Abies* PAR value was the highest compared to all other sites (5,000
28
29 445 grains $\text{cm}^{-2} \text{yr}^{-1}$). PAR values for *Notholithocarpus* and TCT varied across sites and were
30
31 446 between 1,000-4,000 grains $\text{cm}^{-2} \text{yr}^{-1}$.

32
33 447 The group of less abundant arboreal taxa included *Alnus*, *Abies*, and *Quercus* which were
34
35 448 present in most samples with PARs of less than 2,000 grains $\text{cm}^{-2} \text{yr}^{-1}$ (Fig. 5). *Alnus* values were
36
37 449 generally around 1,000 grains $\text{cm}^{-2} \text{yr}^{-1}$, although values above 2,000 grains $\text{cm}^{-2} \text{yr}^{-1}$ were
38
39 450 observed at Ogaromtoc and Fish Lakes. *Abies* values were low ($< 1,000$ grains $\text{cm}^{-2} \text{yr}^{-1}$) at all
40
41 451 sites except North Twin and Onion Lakes. Although pollen from *Alnus*, *Abies*, and *Quercus* were
42
43 452 found at all sites, the taxa themselves were not recorded from the transect sampling at several
44
45 453 lakes. This could be due to low abundance such that they were not captured in the survey or due
46
47 454 to their absence in the pollenshed sedimentary basin in which case their PAR contributions are
48
49 455 background deposition. Pollen from the “other hardwood” category (defined as willows,
50
51 456 buckthorn, hazel, and silk tassel) was detected in trace amounts (< 100 grains $\text{cm}^{-2} \text{yr}^{-1}$).
52
53 457

1
2
3
4
5
6
7
8
9
10
11
12
13
14
15
16
17
18
19
20
21
22
23
24
25
26
27
28
29
30
31
32
33
34
35
36
37
38
39
40
41
42
43
44
45
46
47
48
49
50
51
52
53
54
55
56
57
58
59
60

458 4.3 aRSAP and tRSAP

459 Using the sub-setting approach for the aRSAP calculation, a coherent pattern was exhibited in
460 the likelihood function scores from model 3. The values were high at short distances and then
461 decreased rapidly until 175 m where they begin to flatten out. For all taxa combinations, we
462 inferred via visual inspection that the curves reached their asymptotes at a distance of 625 m and
463 thus the aRSAP of these lakes is 625 m from the lake shore. The likelihood function scores in
464 relation to the distance from the lake shore are shown for one of the three sub-set examples:
465 TCT, *Pseudotsuga*, and *Pinus* (Fig. 6).

466 Based on tRSAP calculations for the four dominant tree taxa, maximum R^2 values were
467 reached before the maximum distance surveyed (750 m) from the shoreline (Fig. 7). The R^2
468 values for *Pinus* and TCT were high (> 0.75) at only 25 m from the shore and stabilized around
469 225 m, the tRSAP. The R^2 values for *Pseudotsuga* and *Notholithocarpus* continued to improve
470 for some distance from the lake shore. For *Pseudotsuga*, the tRSAP was 625 m; for
471 *Notholithocarpus*, it was 525 m. Sample sizes were insufficient to estimate tRSAP values for the
472 minor taxa. For these taxa, we used the aRSAP value in AGL_{dw} calculations (i.e., 625 m).

474 4.4 Transfer functions: PAR to AGL_{dw}

475 PAR was a statistically meaningful and reasonably precise ~~reliable~~ estimator of contemporary
476 AGL_{dw} for most of the pollen taxa present (Fig. 8). Based on the aRSAP distances, the linear
477 model without intercept was the best performing model ($\Delta AIC_c > 4.0$) for the four most
478 abundant taxa (Fig. 8a). For these taxa, the no-intercept regressions were not only significantly
479 better than the null model ($p < 0.001$) but also explained most of the variation. R^2 ranged from
480 0.87 for TCT to 0.96 for *Pseudotsuga* (Table S11). The model results for the three less abundant

1
2
3
4
5
6
7
8
9
10 481 species (i.e., *Alnus*, *Abies* and *Quercus*) were more complex (Fig. 8b). Based on ΔAIC_c , the
11 482 segmented regression model best fit the *Alnus* and *Abies* data. However, both species were rare
12
13 483 and found in abundance at only one lake (Fig. 5). The existence of this one abundant point exerts
14
15 484 extraordinary leverage in the segmented regression. To avoid relying on a single point in these
16
17 485 two transfer functions, we used the second-best regression model. For *Alnus*, it was a linear
18
19 486 model; for *Abies*, it was a linear model without intercept (Table S11). For *Quercus*, none of the
20
21 487 regression models were superior to the null (Fig. 8b, Table S11), so we used the mean and
22
23 488 standard error to predict *Quercus* contribution to AGL_{dw} estimates for each lake. We recalculated
24
25 489 the biomass transfer functions using the tRSAP weighted AGL_{dw} estimates for all taxa. Both the
26
27 490 functional forms and fits were similar to aRSAP-based results (Table S12). However, the
28
29 491 coefficients varied with changes in the source area distance.

30
31 492 The transfer functions based on aRSAP distances provide robust means to estimate
32
33 493 contemporary AGL from PAR (Table 32). The coefficient of variation (COV) in predicted
34
35 494 AGL_{dw} ranged from 13-17% for six lakes with Ogaromtoc being the exception with a COV =
36
37 495 24%. The standard error of the estimate varied little among lakes and averaged 32 Mg ha⁻¹. In
38
39 496 terms of accuracy the relative root mean squared error (rRMSE) between predicted and observed
40
41 497 AGL_{dw} was 9.2%. There was a small tendency for predicted AGL_{dw} to overestimate the
42
43 498 observed. The mean bias was 4.8% with two lakes, Red Mountain and South Twin, contributing
44
45 499 the most to the positive bias (Table 23). The predictions of AGL weighted using tRSAP
46
47 500 distances (Table 34) tended to less accurate (rRMSE = 12.7%) and more biased (10.1%).

501

502 Discussion

503 5.1 Source areas of pollen: aRSAP and tRSAP

1
2
3
4
5
6
7
8
9
10
11
12
13
14
15
16
17
18
19
20
21
22
23
24
25
26
27
28
29
30
31
32
33
34
35
36
37
38
39
40
41
42
43
44
45
46
47
48
49
50
51
52
53
54
55
56
57
58
59
60

504 Calibration of pollen-vegetation relationships is only effective when the scale of the vegetation
505 sampling is close to or exceeds the scale of the relevant source area of pollen (Bunting et al.
506 2004). Therefore, being able to specify the source area of pollen in a given basin is an important
507 step towards quantitative reconstruction of past vegetation (Sugita et al. 1999, Hellman et al.
508 2009). A primary aim of this work was to understand the spatial extent represented by the pollen
509 assemblage. We addressed this aim by determining the assemblage-level relevant source area of
510 pollen (aRSAP) obtained from pollen percentage data and ERV analysis and comparing those
511 estimates with the taxon-specific source area of pollen (tRSAP) for four main taxa. Both metrics
512 estimate the extent of vegetation that requires surveying for a subsequent reconstruction step but
513 are seldom compared.

514 aRSAP values have been estimated for lakes similar in size to those presented here (i.e.,
515 100 m radius), in different settings including simulated landscapes. Reported aRSAP values have
516 ranged from: 300 m in a simulation of a hemlock-hardwood forest in the US (Sugita 1994), to
517 800-1,000 m in a simulation of spruce forest in Sweden (Sugita et al. 1999), to 1,700 m in
518 varying landcover types in Denmark (Nielsen and Sugita 2005), to 1,500-2,000 m in semi-boreal
519 forests of Estonia (Poska et al. 2011), and to 2,200 m in the upper Tibetan Plateau (Wang and
520 Herzs Schuh 2011). Within this list, all aRSAP estimates were derived from Prentice-Sugita-Sutton
521 distance-weighted models and are thus comparable to our estimate. Our aRSAP value of 625 m
522 falls in the range (300-2,200 m), though on the small end.

523 The aRSAP is unique to a given set of lakes and is sensitive to numerous factors such as
524 lake size and basin shape (Sugita 1993), vegetation patch size (Sugita 1994, Broström et al.
525 2005), vegetation patterns (Bunting et al. 2004), and taxa spatial distribution (Hellman et al.
526 2009). For example, aRSAP values tend to increase with landscape openness defined as the

1
2
3
4
5
6
7
8
9
10 527 extent of the vegetation cover in the pollenshedsedimentary basin. For example, the aRSAP for
11 528 small ponds in a closed forest was simulated to be 300 m (Sugita 1994) and empirically verified
12
13 529 by Calcote (1995), whereas the aRSAP for small ponds in an open Swedish landscape was 1,000
14
15 530 m (Sugita et al. 1999). However, expectations based on landscape openness can be complicated
16
17 531 by vegetation heterogeneity. Higher vegetation diversity and complex spatial distribution of taxa
18
19 532 are associated with larger aRSAPs (Hellman et al. 2009). The presence of rare taxa in a
20
21 533 landscape can also increase the aRSAP, other factors being held constant (Bunting et al. 2004).
22
23 534 For example, Commerford et al. (2013) observed the effect of rare taxa empirically: small lakes
24
25 535 in a 'very open' grassland in Kansas had a large aRSAP of 1,060 m, which they attributed to
26
27 536 scattered tree taxa in the tallgrass prairie.

27 537 The contemporary forests around our lake sites are dense, closed, and heavily dominated
28
29 538 by Douglas-fir (Skinner et al. 2018). Taxa like black oak (*Quercus*), white alder (*Alnus*), and
30
31 539 white fir (*Abies*) are present but not common. These rare taxa in the pollenshed-area contributed
32
33 540 little to the overall biomass (2.3%) but make the landscape more heterogeneous. This
34
35 541 heterogeneity can result in a larger aRSAP than if there were no rare taxa present. All else being
36
37 542 equal, longer distances from each sampling site are required to get a sufficient cover of all taxa
38
39 543 within the landscape to reach the regional average. These greater distances produce larger
40
41 544 aRSAP estimates (Hellman et al. 2009).

41 545 tRSAPs have been estimated at small lakes and ponds. For example, the tRSAP for *Pinus*
42
43 546 was 200 m from the lakeshore in southern-northeastern Germany (Matthias and Giesecke 2014),
44
45 547 and other tRSAP values in that study ranged from 50 m (*Quercus*) to 300 m (*Fagus*) to 1,000 m
46
47 548 (*Betula*). Jackson (1990) found small tRSAP estimates from ponds in New York: *Acer* (< 20 m),
48
49 549 *Betula* (> 1,000 m), *Fagus* (> 1,000 m), *Picea* (< 100 m), *Quercus* (> 1,000 m) and *Pinus/Tsuga*

1
2
3
4
5
6
7
8
9
10 550 (< 500 m). In this study, the tRSAP value for *Pinus* was 225 m, a near match to Matthias and
11 551 Giesecke (2014) and comparable to Jackson (1990). The other tRSAP values in this study ranged
12 552 from 225 m (TCT) to 525 m (*Notholithocarpus*) to 625 m (*Pseudotsuga*). Like Matthias and
13 553 Giesecke's results, the tRSAPs are inconsistent with expectations based solely on the respective
14 554 fall speeds of the taxa. For example, *Pinus* has one of the assemblage's lowest fall speeds and
15 555 was expected to travel longer distances and have a large tRSAP; in fact, it had one of the shortest
16 556 tRSAPs.

17
18
19
20
21
22 557 Unexpectedly small source areas of highly dispersible taxa have been observed in
23 558 simulated landscapes (e.g., *Betula*, Sugita 1994) and have been attributed to vegetation
24 559 patterning. The estimated RSAP reflects the minimum distance at which the regional vegetation
25 560 composition is attained. For example, if *Betula* is uniformly spread in a forest, the regional
26 561 distribution signal of *Betula* will be captured closer to the sampling point than in a forest where
27 562 *Betula* is heterogeneously spread across the forest.When a taxon has a relatively homogeneous
28 563 distribution across the landscape (e.g., found in all communities with small patch size, occurs
29 564 frequently as individuals in all communities), the regional distribution of the taxon is attained
30 565 relatively close to the sampling point (e.g., the lake); thus, the vegetation composition does not
31 566 change with increasing distance beyond that point and the source area is small. In this case,
32 567 tRSAP reflects the distance at which regional vegetation composition is reached, instead of being
33 568 predominantly controlled by the taxon's pollen dispersal ability and depositional properties
34 569 (Sugita 1994). The vegetation patterns in the Klamath area are complex and heterogeneous
35 570 (Skinner et al. 2018). Within the sampling area, Douglas-fir (*Pseudotsuga*) is the dominant
36 571 species with large amounts of tanoak (*Notholithocarpus*) at most lake sites, with pines (*Pinus*)
37 572 intermixed and some cedars (TCT). The small "patches" of pines and cedars within a Douglas-fir

1
2
3
4
5
6
7
8
9
10 573 dominant overstory could effectively shrink the tRSAPs of *Pinus* and TCT, following the logic
11 574 presented in Sugita (1994). Thus, the finding of relatively small tRSAPs for *Pinus* and TCT,
12
13 575 despite their fall speeds, and relatively large tRSAPs for *Pseudotsuga* and *Notholithocarpus*,
14
15 576 aligns with the study area's vegetation patterning.

16
17 577 Our estimated aRSAP (625 m) and tRSAP values (all 625 m or less) suggest consistent,
18 578 though not identical, interpretations of the pollenshedsource area of pollen. Both estimates
19
20 579 indicate that the pollen record "senses" a local view of about the same area of the surrounding
21
22 580 vegetation. Given that vegetation surveying must meet or exceed the scale of the relevant source
23
24 581 area of pollen for quantitative reconstruction (Bunting et al. 2004), vastly different aRSAP and
25
26 582 tRSAP estimates would potentially be consequential. If, for example, we had estimated an
27
28 583 aRSAP << tRSAP, it would imply that our assemblage-level view was in some way blind to taxa
29
30 584 in the assemblage, and thus missing important landscape patterning or other features of the
31
32 585 pollenshedarea from which pollen originated. On the other hand, if we had estimated an aRSAP
33
34 586 >> tRSAP, it would imply the subsequent reconstruction represents a larger area than is
35
36 587 potentially being recorded by the pollen system.

37
38 588 This consistency between the aRSAP and tRSAP results was reflected in the similarity of
39
40 589 the AGL_{dw} reconstructions (Table 32, Table 34). On average, observed AGL_{dw} for each lake was
41
42 590 10.1 Mg ha⁻¹ (5.2%) larger using aRSAP with the differences ranging from 2.6 Mg ha⁻¹ (1.1%)
43
44 591 larger at North Twin Lake to 22.2 Mg ha⁻¹ (10.3%) larger at Onion Lake. The differences in
45
46 592 terms of predictive ability were equally modest with aRSAP estimates producing somewhat more
47
48 593 accurate and less biased results.

49
50
51
52 594
53 595 5.2 The potential of calibrated PAR as a bioproxy

1
2
3
4
5
6
7
8
9
10
11
12
13
14
15
16
17
18
19
20
21
22
23
24
25
26
27
28
29
30
31
32
33
34
35
36
37
38
39
40
41
42
43
44
45
46
47
48
49
50
51
52
53
54
55
56
57
58
59
60

596 Establishing the relationship between contemporary biomass and modern PAR values is
597 contingent upon obtaining accurate sedimentation rates in cores. We are confident in our
598 estimated sedimentation rates for two key reasons. First, we used a state of the art, robust
599 Bayesian model to develop age models from ^{210}Pb dates (Aquino-López et al. 2018). Our results
600 showed low uncertainty in the modeled ages in all cores, particularly in the top 20cm. Second,
601 we were able to compare our upper sedimentation rates representing the last decade to estimates
602 from two of the same lakes (Ogaromtoc and Fish lakes) that were collected in 2008 and 2009
603 (Crawford et al. 2015). We found similar sedimentation rates in the upper sediments: 2.0-4.0 mm
604 yr^{-1} compared to 2.0-3.3 mm yr^{-1} . Our modern PAR values are also in agreement with PAR
605 values from the youngest sediments in Crawford et al. (2015).

606 The ultimate goal of this research was to assess whether PAR be used to predict distance-
607 weighted biomass for major tree taxa in the Klamath area, and therefore generate models suitable
608 for reconstruction of past biomass dynamics. The fact that contemporary pollen influx is a
609 reasonably reliable predictor of contemporary distance-weighted AGL at these sites
610 suggests that PAR can be used to infer changes in plant biomass at-for these sites. But even with
611 apparently statistically sound modern models, it may not be reasonable to apply the models for
612 reconstruction in all contexts.

613 In an ideal situation, the calibration dataset would include sites with a wide range of
614 population sizes of the main taxa to allow any time in the fossil record to be reconstructed. Our
615 model had less skill in estimating low levels of forest biomass because we were unable to find
616 lake sites that met our selection criteria and supported sparse forest cover. Other modern
617 quantitative vegetation reconstruction models have been restricted at the upper end of the
618 calibration. Trees growing in dense forest stands produce less pollen than an exposed tree in a

1
2
3
4
5
6
7
8
9
10 619 field, which suggests that increased forest density could result in reduced net pollen productivity
11 620 (Andersen 1970, Fægri and Iverson 1989, Feldman et al. 1999). For example, Blarquez et al.
12
13 621 (2011) found that the relationship between needle accumulation rate and forest basal area tended
14
15 622 to saturate above 40 m² ha⁻¹ for conifer-dominated sites. However, despite the high biomass-
16
17 623 density of the contemporary forest at our sites (Knight et al. 2020), there was no evidence of
18
19 624 saturation in the PAR-biomass functions for the major taxa. Even at the maximum PAR values,
20
21 625 the biomass values increase at pace following the log-linear fits (Fig. 8a).

22 626 Long-term PAR records from lakes in the area provide insight into time periods where
23
24 627 our calibrated models will be able to capture past conditions. Comparable taxa-specific PAR
25
26 628 values from lake sites in the region were only available for *Pinus*, and they suggest time periods
27
28 629 of agreement with our *Pinus* PAR measurements and our total *Pinus* PAR-AGL model, which
29
30 630 covers a range between 1,500 and 11,000 grains cm⁻² yr⁻¹. For example, Briles et al. (2008)
31
32 631 reported *Pinus* PAR between 2,000 and 8,000 grains cm⁻² yr⁻¹ at Sanger Lake in the western
33
34 632 Klamath Mountains over 15,000 years BP. Likewise, a 3,000-year PAR record from Fish Lake (a
35
36 633 lake also examined in this study) shows agreement with our total *Pinus* PAR range during some
37
38 634 time periods. Fish Lake's record shows temporal variability in total *Pinus* PAR values between
39
40 635 2,000 to 9,000 grains cm⁻² yr⁻¹ during the last two hundred years (Crawford et al. 2015), which
41
42 636 falls within our calibration. Lastly, total PAR values measured at eight lakes in the Klamath area
43
44 637 since 15,000 BP range from 2,000 to 15,000 grains cm⁻² yr⁻¹ (Briles et al. 2011) and are similar
45
46 638 in size to lakes in this study and have a dense surrounding forest, although they are located in the
47
48 639 white-fir vegetation zone.

49
50
51
52 640 In addition to selecting a range of forest conditions, researchers undertaking similar
53
54 641 efforts will need to consider the number of lakes needed for statistical soundness for the
55
56
57
58
59
60

1
2
3
4
5
6
7
8
9
10
11
12
13
14
15
16
17
18
19
20
21
22
23
24
25
26
27
28
29
30
31
32
33
34
35
36
37
38
39
40
41
42
43
44
45
46
47
48
49
50
51
52
53
54
55
56
57
58
59
60

642 calibration. The seven lakes presented here appear to have been sufficient to build robust models
643 in terms of low coefficient of variation (Table 23), but it may be difficult in other locations to
644 find enough suitable lakes using consistent selection criteria. If reconstructions of continuous
645 Holocene-length biomass records are sought, using a high number of lakes has the downside of
646 great expense (from isotopic dating) and labor (from pollen counting), unless accurate automatic
647 classification systems become widespread (Sevillano et al. 2020).

648 The calibration step we undertook required modern biomass data, which may be difficult
649 to obtain empirically for a large number of lakes or in settings with challenging topography. For
650 example, transects in this study ran 750 m from the shoreline, but steep topography and scree
651 slopes occasionally prevented a complete survey. Because we studied small lakes and needed
652 finely resolved biomass data, sparse inventory data with large geographic extent (e.g., FIA data)
653 were not an appropriate substitute for field surveys. However, FIA data provided essential
654 information regarding the basal area to biomass relationships for the common tree species in the
655 region (Table S8).

656 *5.3 Limitations of PAR and PVMs*

657 Our results show the utility of calibrated PAR-AGL models for this study, and we have provided
658 a robust process for including uncertainty in PAR-AGL models. However, PAR itself may vary
659 in ways that reduce its value for pollen-based reconstructions in all landscapes. For instance, net
660 pollen deposition can vary spatially and temporally if sediment focusing or pollen redeposition
661 occurs. While studies investigating PAR from modern sedimentary records did not find that
662 redeposition and sediment focusing affected PAR (Seppä and Hicks, 2006; Giesecke and
663 Fontana, 2008), other studies have documented the influence of these factors on PAR (Davis et
664 al. 1984, Odgaard 1993, Matthias and Giesecke 2014). Additionally, between-lake differences in

1
2
3
4
5
6
7
8
9
10 665 PAR values can arise from differences in pollen taphonomy due to basin size or stream inflow
11 666 (Davis 1967b). Pollen monitoring studies have illustrated another known issue with PAR: the
12 667 amount of pollen produced can change year to year and is related to the weather conditions of the
13 668 preceding year (Hicks 2006). Lastly, one study has implied that PAR may depend on the net
14 669 primary production of the pollen-producing taxa as well as overall plant biomass (Matthias and
15 670 Giesecke 2014). Without long-term pollen monitoring studies across different biomes and
16 671 accompanying detailed biomass data, true data validation will not be possible.

17 672 Pollen transport in mountain environments has been studied in Europe through the European
18 673 Pollen Monitoring Programme, but, to our knowledge, has not been studied in the mountains of
19 674 western North America outside of the present work. Several pollen monitoring studies with
20 675 transects running through multiple vegetation zones in mountainous areas tend to show that
21 676 pollen from lower forest zones is quite abundant in upper zones, and this effect appears more
22 677 pronounced when high altitude zones have lower productivity (e.g., the Rila Mountains in
23 678 Bulgaria, Tonkov et al. 2001). Unlike mountain transect studies, our sites are all within one
24 679 vegetation zone, therefore reducing the significance of these effects, and we are not studying tree
25 680 line position. The Douglas-fir dominated conifer forest in the Klamath Mountain is a relatively
26 681 high productivity zone, and such zones typically show less of an “uphill” effect that impacts tree-
27 682 line pollen assemblages (e.g., Swiss Alps tree line study, Sjögren et al. 2008).”

28
29
30
31
32
33
34
35
36
37
38
39
40
41 683 All PVMs, including PAR-biomass transfer functions, are based on assumptions that may not
42 684 hold in a changing landscape. It must be assumed, for example, that taphonomic processes
43 685 filtering pollen in lake sediments are constant over time and among lakes, unless taphonomic
44 686 biases are precisely quantified (Allison and Bottjer 2011). Using our method, quantitative
45 687 biomass reconstruction would also assume that the relevant source area of pollen is constant over
46
47
48
49
50
51

Commented [MOU5]: Added discussion of mountain pollen transport for Reviewer 2.

1
2
3
4
5
6
7
8
9
10
11
12
13
14
15
16
17
18
19
20
21
22
23
24
25
26
27
28
29
30
31
32
33
34
35
36
37
38
39
40
41
42
43
44
45
46
47
48
49
50
51
52
53
54
55
56
57
58
59
60

688 time. We estimated the aRSAP of our seven sites as well as the tRSAP of abundant taxa, but
689 these may apply to a landscape arrangement which is unique in the last 3,000 years. The present-
690 day high PAR values of *Pseudotsuga* are not replicated in the fossil pollen record at any other
691 time in three millennia (Crawford et al. 2015), suggesting that the dominance of shade tolerant
692 *Pseudotsuga* is also not found elsewhere in this time period. Deep-time reconstructions from
693 lakes in this study have shown large changes in vegetation composition due to climate, Native
694 land-use, fire disturbances, and, in the last century, fire suppression. In response, we anticipate
695 that the relevant source areas of pollen will expand and contract over time. Because the spatial
696 patterns of past vegetation are usually unknown, it is difficult to estimate past relevant pollen
697 sources areas. However, the Multiple Scenario Approach (MSA, Bunting and Middleton 2009)
698 offers insight on this issue. Under MSA, hypothetical landscapes are created via rules for plant
699 placement and environmental parameters, and then pollen assemblages are simulated and
700 compared to known pollen signals to identify probable past vegetation mosaics. Another
701 experimental method to estimate past relevant pollen source area has been explored through
702 modeling (Hellman et al. 2009) where regional vegetation composition and available pollen
703 productivity estimates are available for multiple sites (Sugita 2007b). Hellman et al.'s (2009)
704 simulations suggest relatively robust aRSAP estimates of 1,000 to 2,500 m for small lakes under
705 hypothetical landscapes from southern Sweden where natural and anthropogenic disturbances
706 have occurred during the Holocene. Such simulations provide a means to test the potential
707 robustness of aRSAP in the Klamath area.

708

709 5. Conclusion

1
2
3
4
5
6
7
8
9
10 710 Although methodologically challenging, calibrating PAR-biomass models is an important step
11 711 towards quantitative reconstruction of past vegetation. Our calibration steps included estimating
12 712 the spatial extent represented by the pollen system, comparing two estimates of the
13 712 the spatial extent represented by the pollen system, comparing two estimates of the
14
15 713 ~~pollen~~hedRSAP, and evaluating PAR-AGL models. We found comparable aRSAP and tRSAP
16
17 714 estimates that aligned with expectations given the modern forest's dense, closed conditions. We
18 715 also demonstrated that PARs of major tree taxa derived from lake sediments are linearly related
19
20 716 to distance-weighted AGL, and our PAR-AGL_{dw} models accurately reconstruct modern lake-
21
22 717 surrounding biomass. According to PAR values from local and regional lakes sites, our modern
23
24 718 models are broad enough to capture a range of forest structures over the last 15,000 years BP.
25
26 719 We therefore conclude that our results prove the utility of calibrated PAR-AGL models for
27 720 quantitative reconstruction of past vegetation.
28
29
30
31
32
33
34
35
36
37
38
39
40
41
42
43
44
45
46
47
48
49
50
51
52
53
54
55
56
57
58
59
60

1
2
3
4
5
6
7
8
9
10
11
12
13
14
15
16
17
18
19
20
21
22
23
24
25
26
27
28
29
30
31
32
33
34
35
36
37
38
39
40
41
42
43
44
45
46
47
48
49
50
51
52
53
54
55
56
57
58
59
60722 **References**

- 723 Allison P and Bottjer DJ (2011) Taphonomy: Bias and process through time. In: Allison PA and
724 Bottjer DJ (eds) *Taphonomy*. Netherlands: Springer, pp.1–17.
- 725 Andersen ST (1970) The relative pollen productivity and pollen representation of north European
726 trees, and correction factors for tree pollen spectra. *Danmarks geologiske*
727 *Undersogelse* 96:1–99.
- 728 ~~Appleby P and Oldfield F (1978) The calculation of lead-210 dates assuming a constant rate of~~
729 ~~supply of unsupported 210Pb to the sediment. *Catena* 5:1–8.~~
- 730 Aquino-López MA, Blaauw J, Christen A, and Sanderson NK (2018) Bayesian Analysis of 210-
731 Pb Dating. *Journal of Agricultural, Biological, and Environmental Studies*
732 23:317-333.
- 733 Blaauw M and Christen JA (2011) Flexible paleoclimate age-depth models using an
734 autoregressive gamma process. *Bayesian Analysis* 6:457–474.
- 735 ~~Baskaran M, Miller CJ, Kumar A et al. (2015) Sediment accumulation rates and sediment~~
736 ~~dynamics using five different methods in a well-constrained impoundment: Case~~
737 ~~study from Union Lake, Michigan. *Journal of Great Lakes Research* 41:607–617.~~
- 738 Bennett KD (1983) Postglacial population expansion of forest trees in Norfolk, UK. *Nature* 303:
739 164–67.
- 740 Bennett KD (1986) The rate of spread and population increase of forest trees during the
741 postglacial. *Philosophical Transactions of the Royal Society of London, Series B*
742 314:523–531.

- 1
2
3
4
5
6
7
8
9
10 743 Blarquez O, Carcaillet C, Elzein TM et al. (2011) Needle accumulation rate model-based
11 744 reconstruction of paleo-tree biomass in the western subalpine Alps. *The Holocene*
12 745 22:579–587.
- 14 746 Briles CE, Whitlock C, and Bartlein PJ (2005) Postglacial vegetation, fire, and climate history of
16 747 the Siskiyou Mountains, Oregon, USA. *Quaternary Research* 64:44–56.
- 18 748 Briles CE, Whitlock C, Bartlein PJ et al. (2008) Regional and local controls on postglacial
19 749 vegetation and fire in the Siskiyou Mountains, northern California, USA.
21 750 *Palaeogeography, Palaeoclimatology, Palaeoecology* 265:159–169.
- 23 751 Briles CE, Whitlock C, Skinner CN et al. (2011) Holocene forest development and maintenance
25 752 on different substrates in the Klamath Mountains northern California, USA.
26 753 *Ecology* 92:590–601.
- 28 754 Broström A, Gaillard M-J, Ihse M et al. (1998) Pollen–landscape relationships in modern
30 755 analogues of ancient cultural landscapes in southern Sweden — a first step
32 756 towards quantification of vegetation openness in the past. *Vegetation History and*
33 757 *Archaeobotany* 7:189–201.
- 35 758 Broström A, Sugita S and Gaillard M-J (2004) Pollen productivity estimates for the
37 759 reconstruction of past vegetation cover in the cultural landscape of southern
38 760 Sweden. *The Holocene* 14:368–381.
- 41 761 Broström A, Sugita S, Gaillard M-J et al. (2005) Estimating the spatial scale of pollen dispersal
42 762 in the cultural landscape of southern Sweden. *The Holocene* 15:252–262.
- 44 763 Bunting MJ, Gaillard M-J, Sugita S et al. (2004) Vegetation structure and pollen source area. *The*
45 764 *Holocene* 14:651–660.

1
2
3
4
5
6
7
8
9
10
11
12
13
14
15
16
17
18
19
20
21
22
23
24
25
26
27
28
29
30
31
32
33
34
35
36
37
38
39
40
41
42
43
44
45
46
47
48
49
50
51
52
53
54
55
56
57
58
59
60

- 765 Bunting MJ, Armitage R, Binney HA et al. (2005) Estimates of 'relative pollen productivity' and
766 'relevant source area of pollen' for major tree taxa in two Norfolk (UK)
767 woodlands. *The Holocene* 15:459–465.
- 768 Bunting MJ and Middleton R (2005) Modelling pollen dispersal and deposition using HUMPOL
769 software: simulating wind roses and irregular lakes. *Review of Palaeobotany and*
770 *Palynology* 134:185–196.
- 771 Bunting MJ and Middleton R (2009) The Multiple Scenario Approach: a pragmatic method for
772 past vegetation mosaic reconstruction. *The Holocene* 19:799–803.
- 773 Bunting MJ and Hjelle KL (2010) Effect of vegetation data collection strategies on estimates of
774 relevant source area of pollen (RSAP) and relative pollen productivity estimates
775 (relative PPE) for non-arboreal taxa. *Vegetation History and Archaeobotany*
776 19:365–374.
- 777 Bunting MJ, Farrell M, Broström A et al. (2013) Palynological perspectives on vegetation
778 survey: a critical step for model-based reconstruction of Quaternary land cover.
779 *Quaternary Science Reviews* 82:41–55.
- 780 Burnham KP and Anderson DR (2002) Model selection and multimodel inference: a practical
781 information-theoretic approach. New York: Springer-Verlag.
- 782 Calcote R (1995) Pollen source area and pollen productivity: evidence from forest hollows.
783 *Journal of Ecology* 83:591–602.
- 784 Cheng STE (2004) *Forest Service Research Natural Areas in California*. General Technical
785 Report PSW-GTR-188. Pacific Southwest Research Station, Forest Service, U.S.
786 Department of Agriculture, Albany, CA.

- 1
2
3
4
5
6
7
8
9
10 787 Christen JA and Fox C (2010) A general purpose sampling algorithm for continuous
11 788 distributions (the t-walk). *Bayesian Analysis* 5:263–281.
- 12
13 789 Colombaroli D and Gavin DG (2010) Highly episodic fire and erosion regime over the past
14
15 790 2,000 years in the Siskiyou Mountains, Oregon. *Proceedings of the National*
16
17 791 *Academy of Sciences* 107:18909–18914.
- 18 792 Commerford JL, McLauchlan KK and Sugita S (2013) Calibrating vegetation cover and
19
20 793 grassland pollen assemblages in the Flint Hills of Kansas, USA. *American*
21
22 794 *Journal of Plant Sciences* 4:1–10.
- 23
24 795 Crawford JN, Mensing SA, Lake FK et al. (2015) Late Holocene fire and vegetation
25
26 796 reconstruction from the western Klamath Mountains, California, USA: A
27
28 797 multidisciplinary approach for examining potential human land-use impacts. *The*
29
30 798 *Holocene* 25:1341–1357.
- 31 799 Crowley PH (1992) Resampling methods for computation-intensive data analysis in ecology and
32
33 800 evolution. *Annual Review of Ecological Systems* 23:405–447.
- 34 801 Daniels ML, Anderson RS and Whitlock C (2005) Vegetation and fire history since the Late
35
36 802 Pleistocene from the Trinity Mountains, northwestern California, USA. *The*
37
38 803 *Holocene* 15:1062–1071.
- 39 804 Davis MB (1963) On the theory of pollen analysis. *American Journal of Science* 261:897–912.
40
41 805 [Davis MB \(1967b\) Pollen deposition in lakes as measured by sediment traps. *Geological Society*](#)
42
43 806 [of America Bulletin 78: 849–58.](#)
- 44
45 807 Davis MB and Deevey ES (1964) Pollen accumulation rates: estimates from Late-Glacial
46
47 808 sediment Rogers Lake. *Science* 145:1293–1295.
- 48
49
50
51
52
53
54
55
56
57
58
59
60

1
2
3
4
5
6
7
8
9
10
11
12
13
14
15
16
17
18
19
20
21
22
23
24
25
26
27
28
29
30
31
32
33
34
35
36
37
38
39
40
41
42
43
44
45
46
47
48
49
50
51
52
53
54
55
56
57
58
59
60

- 809 Davis MB, Brubaker LB and Webb T (1973) Calibration of absolute pollen influx. In: Birks HJB
810 and West RG (eds) *Quaternary Plant Ecology*. Oxford: Blackwell Scientific
811 Publications, pp.9–25.
- 812 Davis MB, Moeller RE and Ford J (1984) Sediment focusing and pollen influx. In: Haworth EY
813 and Lund JWG (eds) *Lake sediments and environmental history*. Minneapolis:
814 University of Minnesota Press, pp.261–93.
- 815 Davis MB (2000) Palynology after Y2K: Understanding the source area of pollen in sediments.
816 *Annual Review of Earth Planetary Sciences* 28:1–18.
- 817 [Dawson A, Paciorek CJ, Goring SJ, Jackson ST, McLachlan JS, Williams JW \(2019\)](#)
818 [Quantifying trends and uncertainty in prehistoric forest composition in the upper](#)
819 [Midwestern United States *Ecology* 100\(12\):1–18.](#)
- 820 Doher LI (1980) Palynomorph preparation procedures currently used in the paleontology and
821 stratigraphy laboratories. *U.S. Geological Survey Circular* 830:1–28.
- 822 Fægri K and Iversen J (1989) *Textbook of Pollen Analysis*. New York: Haffner Press.
- 823 Fagerlind F (1952) The real significance of pollen diagrams. *Botaniska Notiser* 105:185–224.
- 824 Feldman R, Tomback DF and Koehler J (1999) Cost of mutualism: competition, tree
825 morphology, and pollen production in limber pine clusters. *Ecology* 80:324–329.
- 826 FIADB (2020) Forest Inventory and Analysis Database version 1.8.0.0.1.
827 <https://apps.fs.usda.gov/fia/datamart/datamart.html>
- 828 Gaillard M-J, Sugita S, Broström A et al. (2000) Long term land-cover changes on regional to
829 global scales inferred from fossil pollen — how to meet the challenges of climate
830 research? *Pages Newsletter* 8:30–32.

- 1
2
3
4
5
6
7
8
9
10 831 Gaillard M-J, Sugita S, Mazier F et al. (2010) Holocene land-cover reconstructions for studies on
11 land cover-climate feedbacks. *Climate of the Past* 6:483–499.
12
13 833 Giesecke T (2005) Moving front or population expansion: how did *Picea abies* (L.) Karst.
14 become frequent in central Sweden? *Quaternary Science Reviews* 24:2495–509.
15 834
16 835 [Giesecke T, Fontana SL \(2008\) Revisiting pollen accumulation rates from Swedish lake](#)
17 [sediments. *The Holocene* 18:293-305.](#)
18 836
19
20 837 Gregory PH (1973) *The Microbiology of the Atmosphere*. London: L. Hill Publishers.
21
22 838 Halbritter H, Ulrich S, Grímsson F et al. (2018) *Illustrated Pollen Terminology*. Vienna:
23 Springer International Publishing.
24 839
25 840 Han Y, Liu H, Hao Q et al. (2017) More reliable pollen productivity estimates and relative
26 source area of pollen in a forest-steppe ecotone with improved vegetation survey.
27 841
28 *The Holocene* 27:1567–1577.
29 842
30 843 Hellman S, Gaillard MJ, Broström A et al. (2008a) The REVEALS model, a new tool to estimate
31 past regional plant abundance from data in large lakes: validation in southern
32 844 Sweden. *Journal of Quaternary Science* 23:21–42.
33 845
34 846 Hellman S, Broström A, Gaillard MJ et al. (2008b) Effects of the sampling design and selection
35 of parameter values on pollen based quantitative reconstructions of regional
36 847 vegetation: a case study in southern Sweden using the REVEALS model.
37 848
38 *Vegetation Historical Archaeobotany* 17:445–460.
39 849
40 850 Hellman S, Bunting MJ and Gaillard M-J (2009) Relevant Source Area of Pollen in patchy
41 cultural landscapes and signals of anthropogenic landscape disturbance in the
42 851 pollen record: A simulation approach. *Review of Palaeobotany and Palynology*
43 852
44 153:245–258.
45 853
46
47
48
49
50
51
52
53
54
55
56
57
58
59
60

1
2
3
4
5
6
7
8
9
10
11
12
13
14
15
16
17
18
19
20
21
22
23
24
25
26
27
28
29
30
31
32
33
34
35
36
37
38
39
40
41
42
43
44
45
46
47
48
49
50
51
52
53
54
55
56
57
58
59
60

- 854 [Hicks, S. and Hyvarinen, H. 1999: Pollen influx values measured in different sedimentary](#)
855 [environments and their palaeoecological implications. *Grana* 38:228–42.](#)
- 856 Hicks S (2001) The use of annual arboreal pollen deposition values for delimiting tree-lines in
857 the landscape and exploring models of pollen dispersal. *Review of Palaeobotany*
858 *and Palynology* 117:1–29.
- 859 [Hicks S \(2006\) When no pollen does not mean no trees. *Vegetation History and Archeobotany*](#)
860 [15:253–261.](#)
- 861 Hickman JC (1993) *The Jepson manual: higher plants of California*. Berkeley: University of
862 California Press.
- 863 Hudiburg T, Law B, Turner DP et al. (2009) Carbon dynamics of Oregon and Northern
864 California forests and potential land-based carbon storage. *Ecological*
865 *Applications* 19:163–180.
- 866 Hyvärinen H (1975) Absolute and relative pollen diagrams from northernmost Fennoscandia.
867 *Fennia* 142:1–23.
- 868 Irwin WP (1981) Tectonic accretion of the Klamath Mountains. In: Ernst WG (ed) *The*
869 *Geotectonic Development of California*. Englewood Cliffs: Prentice Hall, pp.29–
870 49.
- 871 Jackson ST (1990) Pollen Source Area and Representation in Small Lakes of the Northeastern
872 United States. *Review of Palaeobotany and Palynology* 63:53–76.
- 873 [Jweda J and Baskaran M \(2011\) Interconnected riverine-lacustrine systems as sedimentary](#)
874 [repositories: Case study in southeast Michigan using \$^{210}\text{Pb}\$ and \$^{137}\text{Cs}\$ sediment](#)
875 [accumulation and mixing models. *Journal of Great Lakes Research* 37:432–446.](#)
- 876 Knapp RO (1969) *How to know pollen and spores*. Minneapolis: W.C. Brown Company.

- 1
2
3
4
5
6
7
8
9
10 877 Knight CA, Cogbill CV, Potts MD et al. (2020) Settlement-era forest structure and composition
11 878 in the Klamath Mountains: Reconstructing a historical baseline. *Ecosphere*
12 879 11:e03250.
- 14
15 880 Likens GE and Davis MB (1975) Post-glacial History of Mirror Lake and its Watershed in New
16 881 Hampshire: an Initial Report. *Internationale Vereinigung für Theoretische und*
17 882 *Angewandte Limnologie* 19:982–993.
- 19
20 883 MacDonald GM (1993) Fossil pollen analysis and the reconstruction of plant invasions.
21 884 *Advances in Ecological Research* 24:67–109.
- 23
24 885 Marquer L, Gaillard M-J, Sugita S et al. (2014) Holocene changes in vegetation composition in
25 886 northern Europe: why quantitative pollen-based vegetation reconstructions
26 887 matter. *Quaternary Science Reviews* 90:199–216.
- 28
29 888 Matthias I and Giesecke T (2014) Insights into pollen source area, transport and deposition from
30 889 modern pollen accumulation rates in lake sediments. *Quaternary Science Reviews*
31 890 87:12–23.
- 33
34 891 Mohr JA, Whitlock C and Skinner CN (2000) Postglacial vegetation and fire history, eastern
35 892 Klamath Mountains, California. *The Holocene* 10:587–601.
- 37
38 893 Morris JL, DeRose JR and Brunelle AR (2015) Long-term landscape changes in a subalpine
39 894 spruce-fir forest in central Utah, USA. *Forest Ecosystems* 2:1–12.
- 41
42 895 Muggeo VM (2008) Segmented: an R package to fit regression models with broken-line
43 896 relationships. *R News* 8:20–25.
- 44
45 897 Nielsen AB and Sugita S (2005) Estimating Relevant Source Area of Pollen for Small Danish
46 898 Lakes around AD 1800. *The Holocene* 15:1006–1020.

1
2
3
4
5
6
7
8
9
10
11
12
13
14
15
16
17
18
19
20
21
22
23
24
25
26
27
28
29
30
31
32
33
34
35
36
37
38
39
40
41
42
43
44
45
46
47
48
49
50
51
52
53
54
55
56
57
58
59
60

- 899 [Odgaard BV \(1993\) Wind-determined sediment distribution and Holocene sediment yield in a](#)
900 [small, Danish kettle lake. *Journal of Paleolimnology* 8:3–13.](#)
- 901 Parsons R and Prentice IC (1981) Statistical approaches to R-values and the pollen vegetation
902 relationship. *Review of Palaeobotany and Palynology* 32:127–152.
- 903 Poska A, Meltsov V, Sugita S et al. (2011) Relative pollen productivity estimates of major
904 anemophilous taxa and relevant source area of pollen in a cultural landscape of
905 the semi-boreal forest zone (Estonia). *Review of Palaeobotany and Palynology*
906 167:30–39.
- 907 Prentice IC (1985) Pollen representation, source area, and basin size: towards a unified theory of
908 pollen analysis. *Quaternary Research* 23:76–86.
- 909 Prentice IC (1988) Records of vegetation in time and space: the principles of pollen analysis. In:
910 Huntley B and Webb T III (eds) *Vegetation history*. Dordrecht: Kluwer Academic
911 Publishers, pp.17–42.
- 912 Ritchie JC (1969) Absolute pollen frequencies and carbon-14 age of Holocene lake sediment
913 from the Riding Mountain area of Manitoba. *Canadian Journal of Botany* 47:
914 1345–1349.
- 915 Sawyer JO and Thornburg DA (1977) Montane and subalpine vegetation of the Klamath
916 Mountains. In: Barbour MG and Major J (eds) *Terrestrial Vegetation of*
917 *California*. Berkeley: California Native Plant Society, pp.699–732.
- 918 Sevillano V, Holt K and Aznarte JL (2020) Precise automatic classification of 46 different pollen
919 types with convolutional neural networks. *PLoS ONE* 15:e0229751.

- 1
2
3
4
5
6
7
8
9
10 920 Seppä H and Hicks S (2006) Integration of modern and past pollen accumulation rate (PAR)
11 921 records across the arctic tree-line: a method for more precise vegetation
12 reconstructions. *Quaternary Science Review* 25:1501–1516.
13 922
14 923 Seppä H, Alenius T, Muukkonen P et al. (2009) Calibrated pollen accumulation rates as a basis
15 924 for quantitative tree biomass reconstructions. *The Holocene* 19:209–220.
16 925 [Sjögren P, van der Knaap WO, Huuskoc A, van Leeuwen JFN \(2008\) Pollen productivity,](#)
17 926 [dispersal, and correction factors for major tree taxa in the Swiss Alps based on](#)
18 927 [pollen-trap results. *Review of Palaeobotany and Palynology* 152:200–210.](#)
19
20
21
22
23 928 Skinner CN, Taylor AH and Agee JK (2006) Klamath Mountains Bioregion. In: Sugihara NG,
24 929 van Wagtenonk JW, Fites-Kaufmann J, Shaffer KE and Thode AE (eds) *Fire in*
25 930 *California's ecosystems*. Berkeley: University of California Press, pp.170–194.
26
27 931 Skinner CN, Taylor AH, Agee JK et al. (2018) Klamath Mountains bioregion. In: van
28 932 Wagtenonk JW, Sugihara NS, Stephens SL, Thode A, Shaffer K, and Fites-
29 933 Kaufmann J (eds) *Fire in California's ecosystems*. Berkeley: University of
30 934 California Press, pp.171–193.
31
32 935 Soepboer W, Sugita S, Lotter AF et al. (2007) Pollen productivity estimates for quantitative
33 936 reconstruction of vegetation cover on the Swiss Plateau. *The Holocene* 17:65–77.
34 937 Stockmarr J (1971) Tablets with spores used in pollen analysis. *Pollen and Spores* 13:615–621.
35 938 Sugita S (1993) A model of pollen source area for an entire lake surface. *Quaternary Research*
36 939 39:239–244.
37 940 Sugita S (1994) Pollen representation of vegetation in Quaternary sediments: Theory and method
38 941 in patchy vegetation. *Journal of Ecology* 82:881–897.
39 942 Sugita S (1998) Modelling pollen representation of vegetation. In: Gaillard M-J and Berglund
40
41
42
43
44
45
46
47
48
49
50
51
52
53
54
55
56
57
58
59
60

1
2
3
4
5
6
7
8
9
10
11
12
13
14
15
16
17
18
19
20
21
22
23
24
25
26
27
28
29
30
31
32
33
34
35
36
37
38
39
40
41
42
43
44
45
46
47
48
49
50
51
52
53
54
55
56
57
58
59
60

- 943 BE (eds) *Quantification of land surfaces cleared of forests during the Holocene –*
944 *modern pollen/vegetation/landscape relationships as an aid to the interpretation*
945 *of fossil pollen data*. Gustav Fischer Verlag, pp.1–18.
- 946 Sugita S, Gaillard M-J and Broström A (1999) Landscape openness and pollen records: a
947 simulation approach. *The Holocene* 9:409–421.
- 948 Sugita S (2007a) Theory of quantitative reconstruction of vegetation I: Pollen from large sites
949 REVEALS regional vegetation composition. *The Holocene* 17:229–241.
- 950 Sugita S (2007b) Theory of quantitative reconstruction of vegetation II: All you need is LOVE.
951 *The Holocene* 17:243–257.
- 952 Sutton OG (1947) The problem of diffusion in the lower atmosphere. *Quarterly Journal of the*
953 *Royal Meteorological Society* 73: 257–276.
- 954 Sutton OG (1953) *Micrometeorology*. New York: McGraw-Hill.
- 955 Swetnam TW, Allen CD and Betancourt JL (1999) Applied historical ecology: Using the past to
956 manage for the future. *Ecological Applications* 9:1189–1206.
- 957 Taylor AH and Skinner CN (2003) Spatial patterns and controls on historical fire regimes and
958 forest structure in the Klamath Mountains. *Ecological Applications* 13:704–719.
- 959 Theuerkauf M, Kuparinen A and Joosten H (2012) Pollen productivity estimates strongly depend
960 on assumed pollen dispersal. *The Holocene* 23: 14–24.
- 961 [Tonkova S, Hicks S, Bozilovaa E, Atanassova J \(2001\) Pollen monitoring in the central Rila](#)
962 [Mountains, Southwestern Bulgaria: comparisons between pollen traps and surface](#)
963 [samples for the period 1993±1999. *Review of Palaeobotany and Palynology*](#)
964 [117:167–182.](#)

- 1
2
3
4
5
6
7
8
9
10 965 United States Department of Agriculture, Forest Service (2000) *Timber Cruising Handbook and*
11 966 *Amendments*. Technical Report FSH 2409.12. Washington, DC, USA.
12
13 967 Von Post L (1918) Skogsträdpollen i sydsvenska torvmosselagerföljder. In: Forhandlingar ved de
14
15 968 skandinaviske naturforskere 16. Møte i Kristiania den 10–15. Juli 1916.
16
17 969 Skandinaviska Naturforskarmöten, Kristiania, pp.432–465
18
19 970 Wahrhaftig C and Birman JH (1965) The Quaternary of the Pacific mountain system in
20 971 California. In: HE Wright and Frey DG (eds) *Quaternary of the United States*.
21
22 972 Princeton: Princeton University Press, pp.299–341.
23
24 973 Wang Y and Herzschuh U (2011) Reassessment of Holocene vegetation change on the upper
25 974 Tibetan Plateau using the pollen-based REVEALS model. *Review of*
26
27 975 *Palaeobotany and Palynology* 168:31–40.
28
29 976 Wanket J (2002) *Late Quaternary vegetation and climate of the Klamath Mountains*. PhD
30 977 Dissertation, University of California, Berkeley, USA.
31
32 978 Whittaker RH (1960) Vegetation of the Siskiyou Mountains, Oregon and California. *Ecological*
33
34 979 *Monographs* 30:279–338.
35
36 980 Zhou X and Hemstrom MA (2009) *Estimating aboveground tree biomass on forest land in the*
37 981 *Pacific Northwest: a comparison of approaches*. PNW-RP-584. US Department
38
39 982 of Agriculture, Forest Service, Pacific Northwest Research Station.
40
41
42
43
44
45
46
47
48
49
50
51

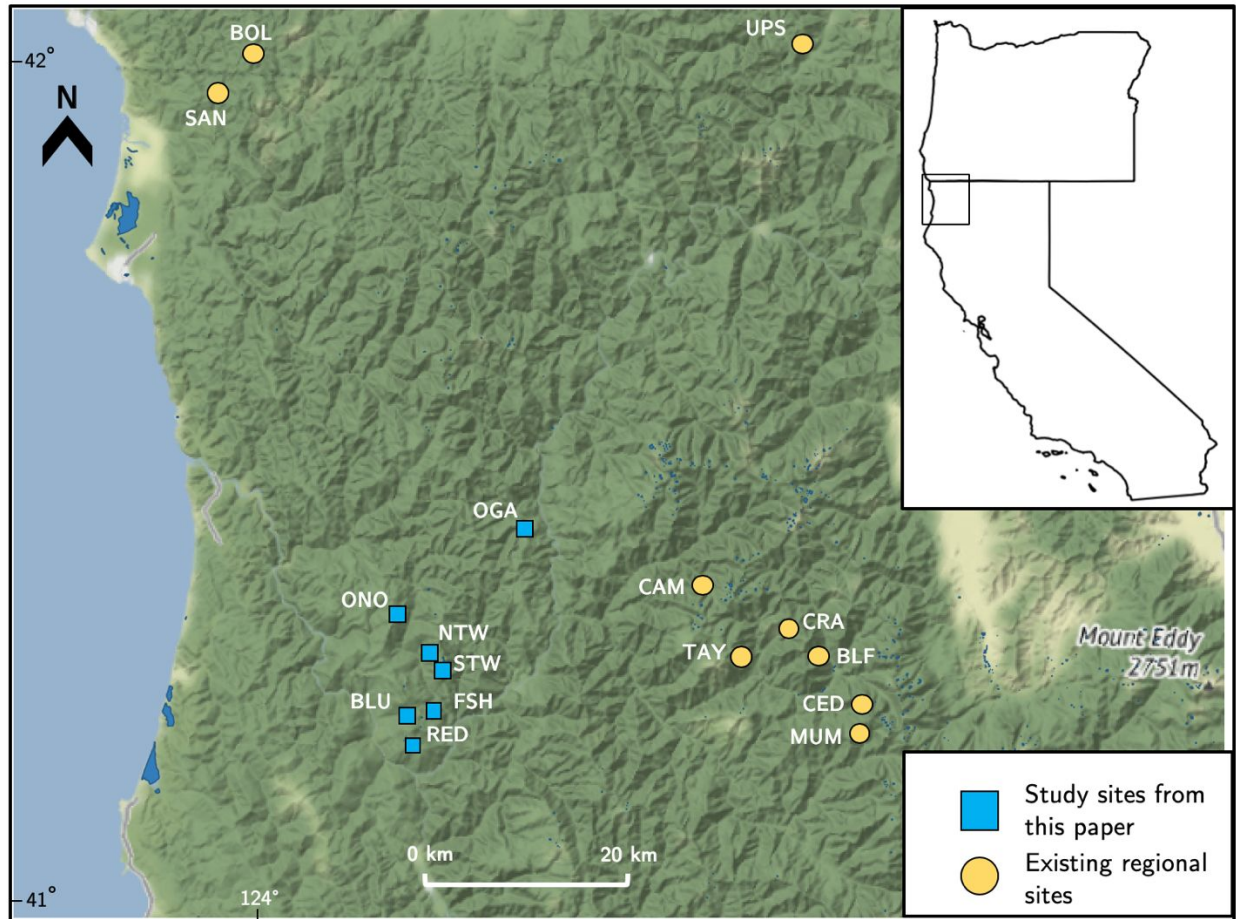


Figure 1. Map shows study sites (blue squares) in northwestern California: Blue Lake (BLU), Fish Lake (FSH), North Twin Lake (NTW), Lake Ogaromtoc (OGA), Onion Lake (ONO), Red Mountain Lake (RED), and South Twin Lake (STW). Note that Lake Ogaromtoc and Fish Lake were described in Crawford et al. (2015) and North and South Twin Lake were described in Wanket (2002) but were also studied in this project. Map also shows Holocene-era pollen records from other parts of the region (yellow circles): Bluff (BLF) and Crater (CRA) Lakes (Mohr et al. 2000); Sanger (SAN) and Bolan (BOL) Lakes (Briles et al. 2008); Upper Squaw Lake (USL; Colombaroli and Gavin 2010); Mumbo (MUM) Lake (Daniels et al. 2005); and Campbell (CAM), Taylor (TAY), and Cedar (CED) Lakes (Briles et al. 2011).

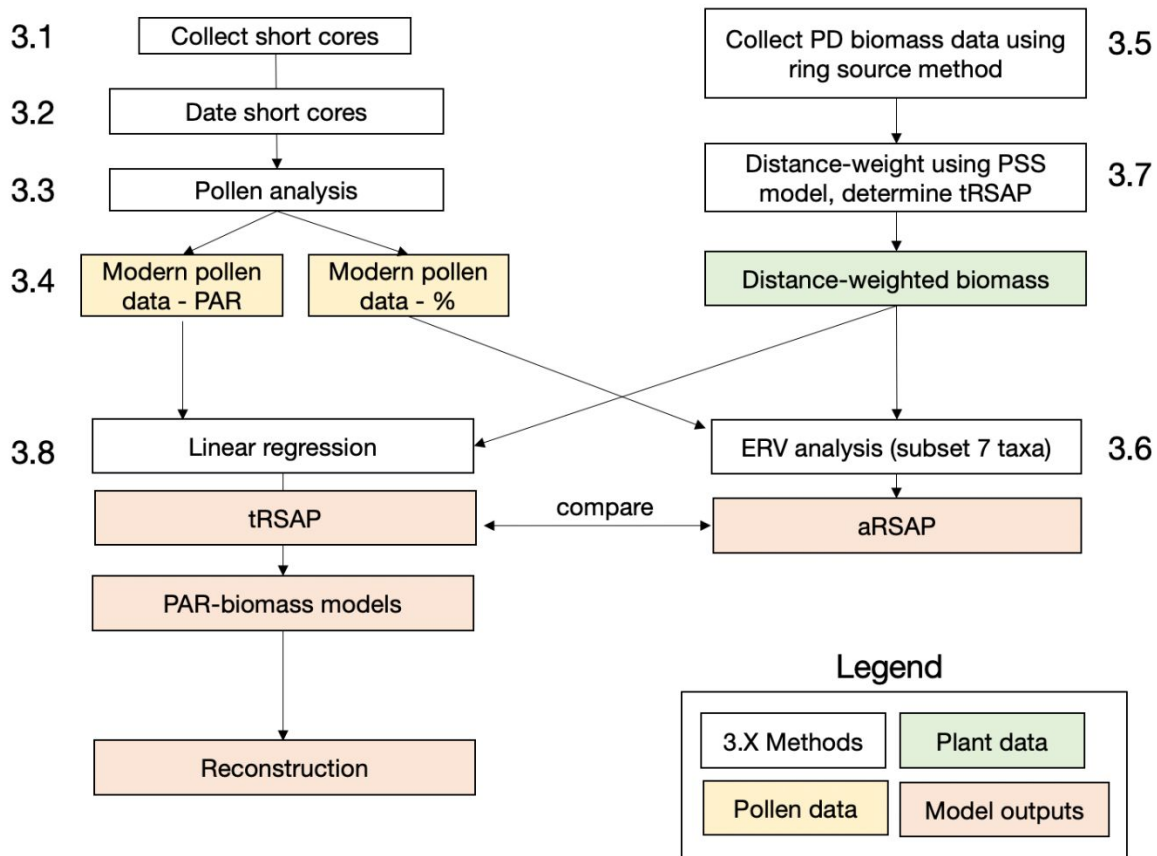


Figure 2. Flowchart of methodological steps leading to a calibrated PAR-biomass model.

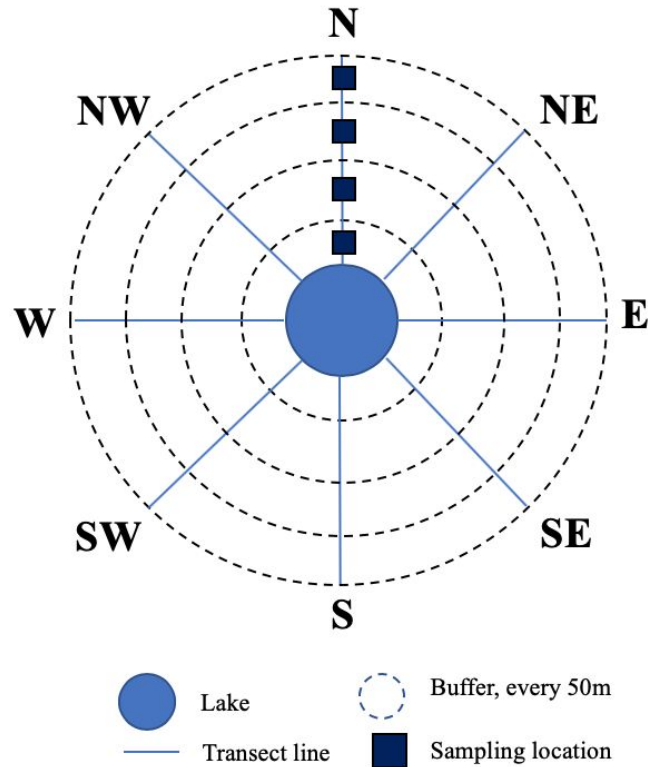


Figure 3. A schematic of the vegetation survey design (not to scale), following Han et al. (2017), that included eight transect lines along the cardinal and sub-cardinal directions where sampling occurred at the mid-point of each concentric ring (the schematic shows an example with only four rings). Sample locations (squares) are shown on the north transect for illustration.

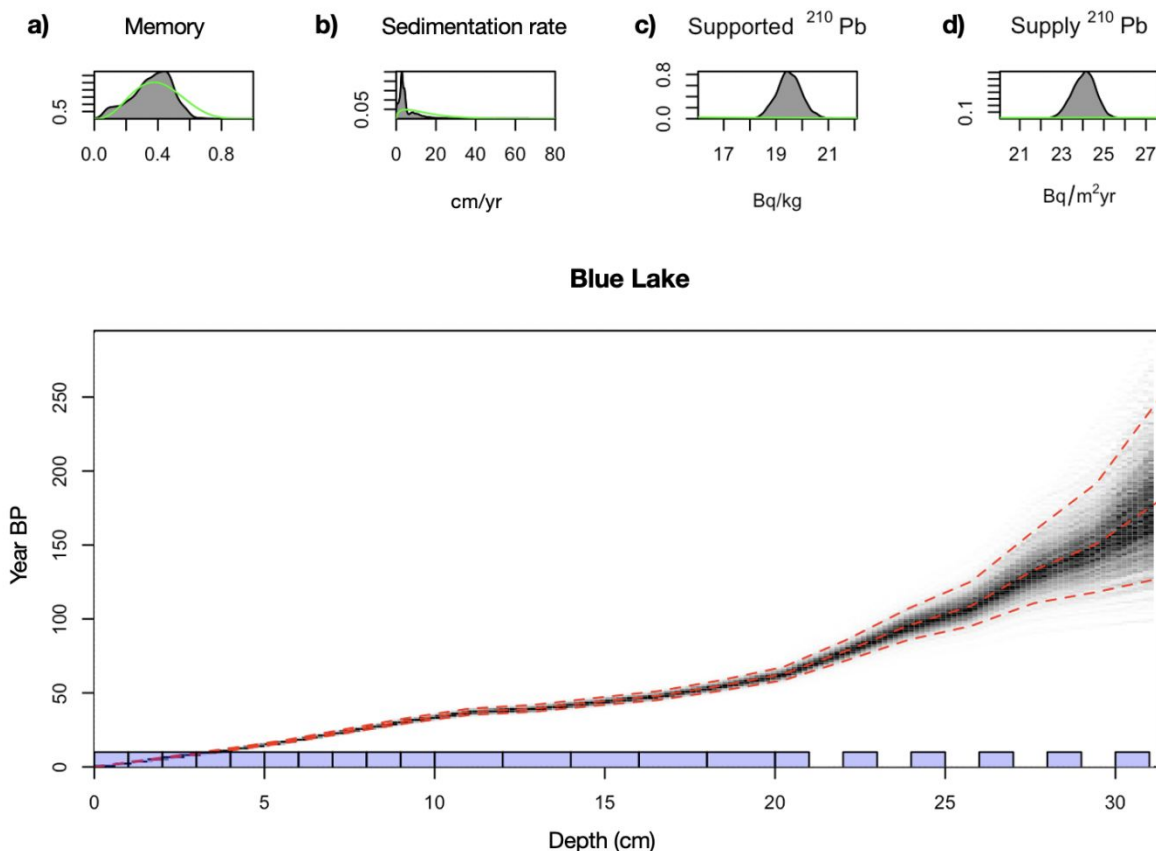


Figure 4. Example of Pb-210 age model construction. The age-to-depth results of the Plum modeling for Blue Lake. The grey lines are simulation from Plum and the dashed red lines represent the mean age and the 95% interval. The small panels at the top show the prior (green) and posterior (grey) distributions for **(a)** the memory (ω), which describes the coherence in sedimentation rates along the core **(b)** the sedimentation rate (α), **(c)** the supported ^{210}Pb (P^S), which is the background level of ^{210}Pb already present in the sediment, and **(d)** and the supply of ^{210}Pb (Φ). For other sites, see Supplementary Information.

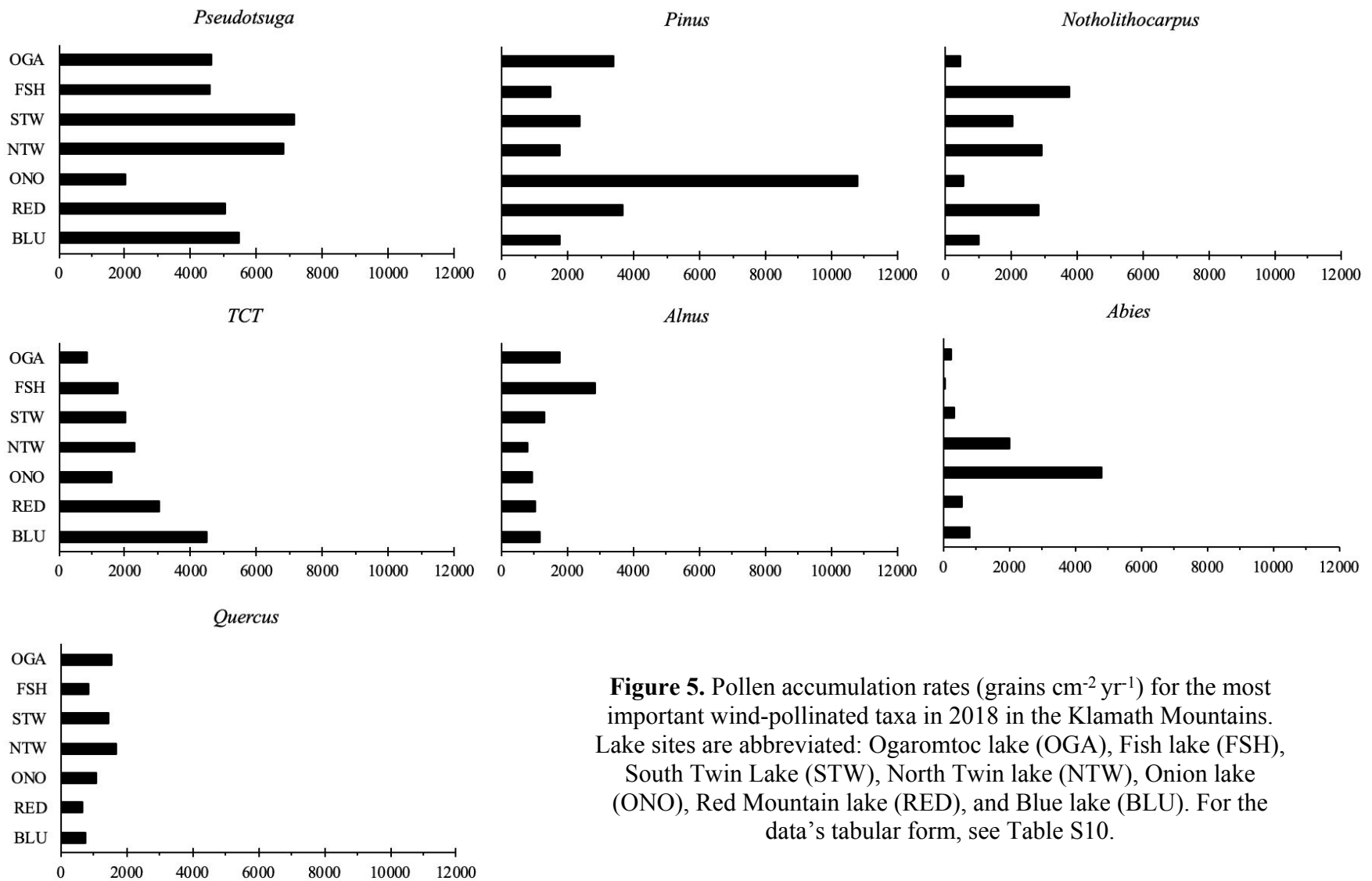


Figure 5. Pollen accumulation rates (grains cm⁻² yr⁻¹) for the most important wind-pollinated taxa in 2018 in the Klamath Mountains. Lake sites are abbreviated: Ogaromtoc lake (OGA), Fish lake (FSH), South Twin Lake (STW), North Twin lake (NTW), Onion lake (ONO), Red Mountain lake (RED), and Blue lake (BLU). For the data's tabular form, see Table S10.

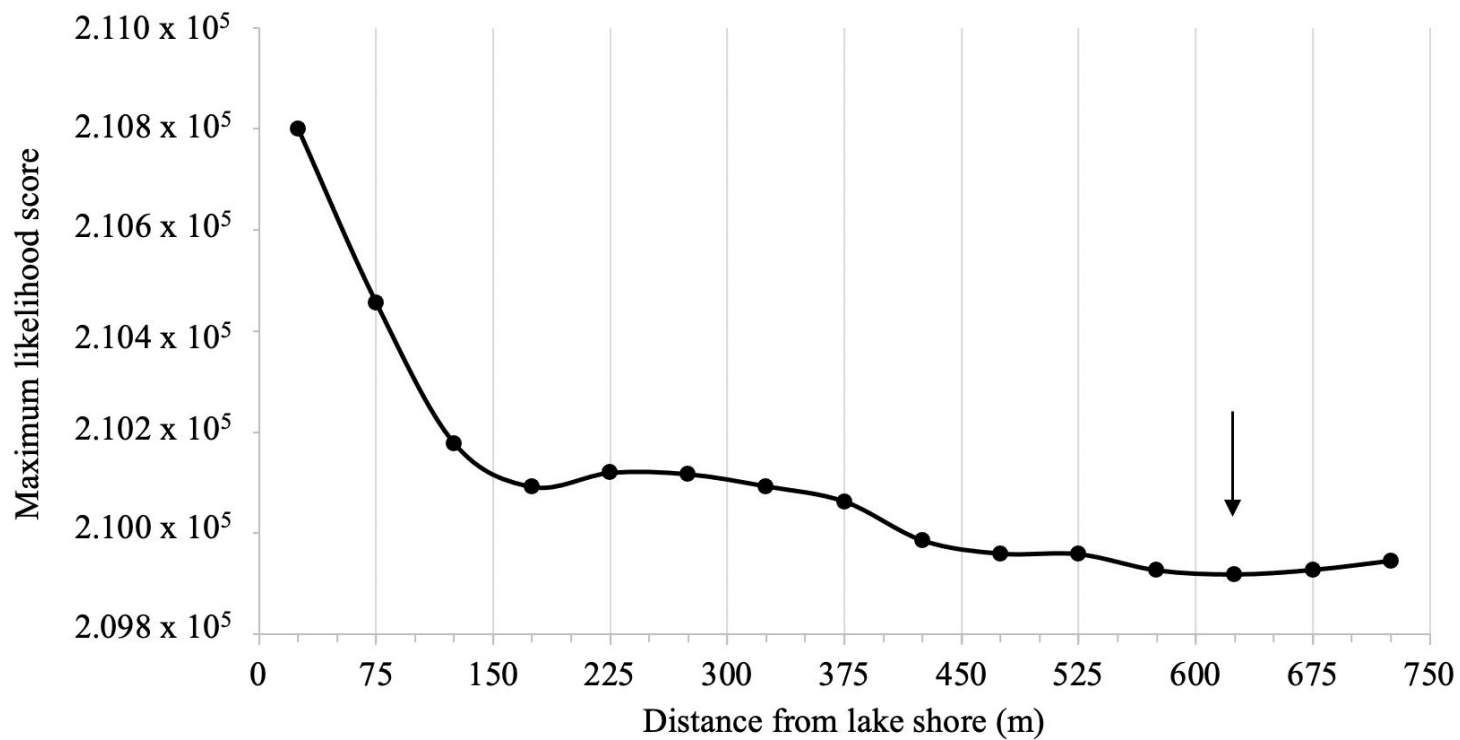


Figure 6. PolERV model 3 results of maximum likelihood scores compared to distance (m). Arrow indicates the aRSAP value (625m).

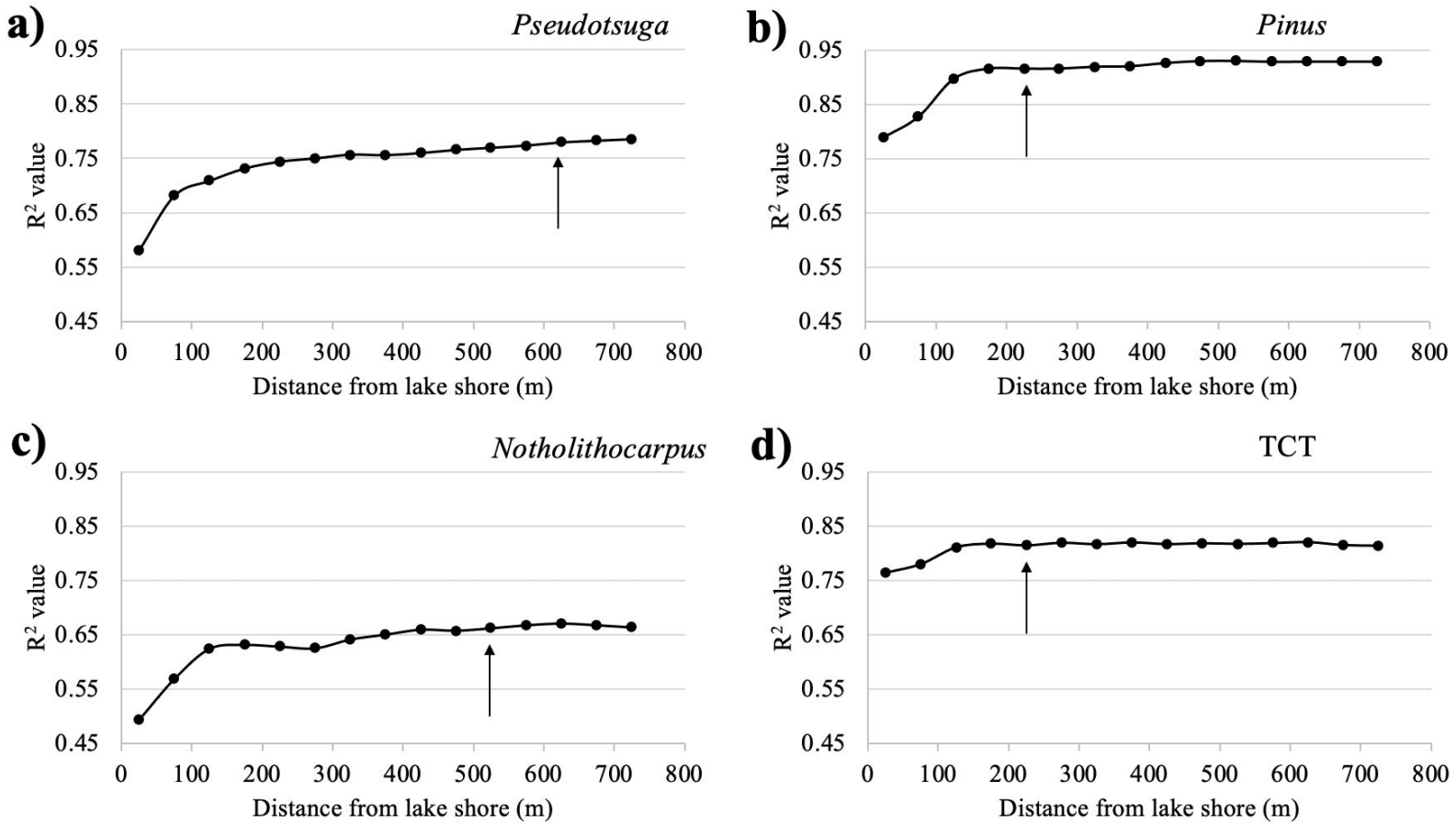


Figure 7. R^2 for regressions between AGL_{dw} and PAR at increasing distance from the lake shore to the furthest vegetation survey site. tRSAP is shown by the arrow: a) *Pseudotsuga* (625m), b) *Pinus* (225m), c) *Notholithocarpus* (525m), and d) TCT (225m).

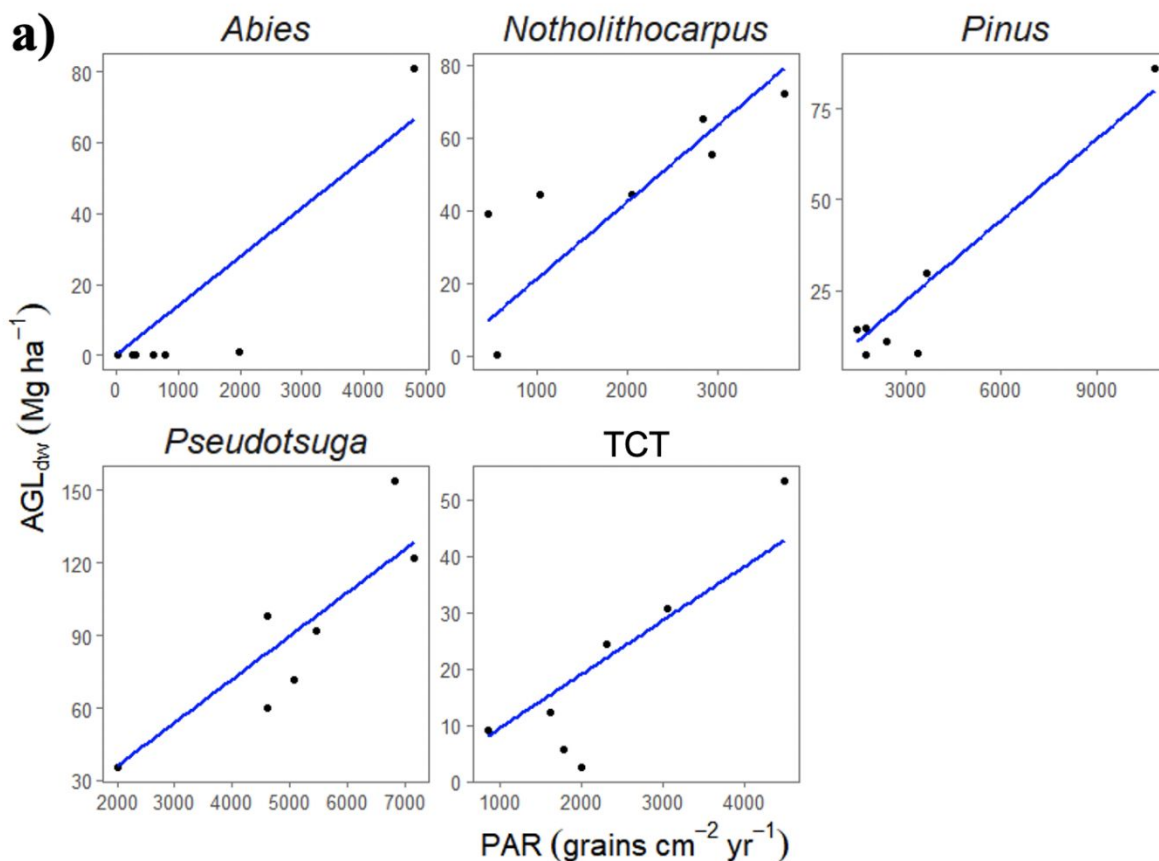


Figure 8a. The relationship between distance-weighted aboveground live biomass (AGL_{DW}) and pollen accumulation rate (PAR) for five of the pollen taxa present at the seven lake sites in the Klamath Mountains. Lines represent linear regressions forced through the origin. The relevant source area of pollen (aRSAP) was defined as a circle with a radius of 625 m from the centroid of the lake. Note that the scales change for each pollen taxa. For summaries of the linear models, see Table S11. (Note: Although biomass “predicts” pollen accumulation rates in a functional sense, our aim is to eventually apply calibrated transfer functions to predict biomass in the past; thus, we fitted regression lines with PAR values as the independent variable.)

1
2
3
4
5
6
7
8
9
10
11
12
13
14
15
16
17
18
19
20
21
22
23
24
25
26
27
28
29
30
31
32
33
34
35
36
37
38
39
40
41
42
43
44
45
46
47

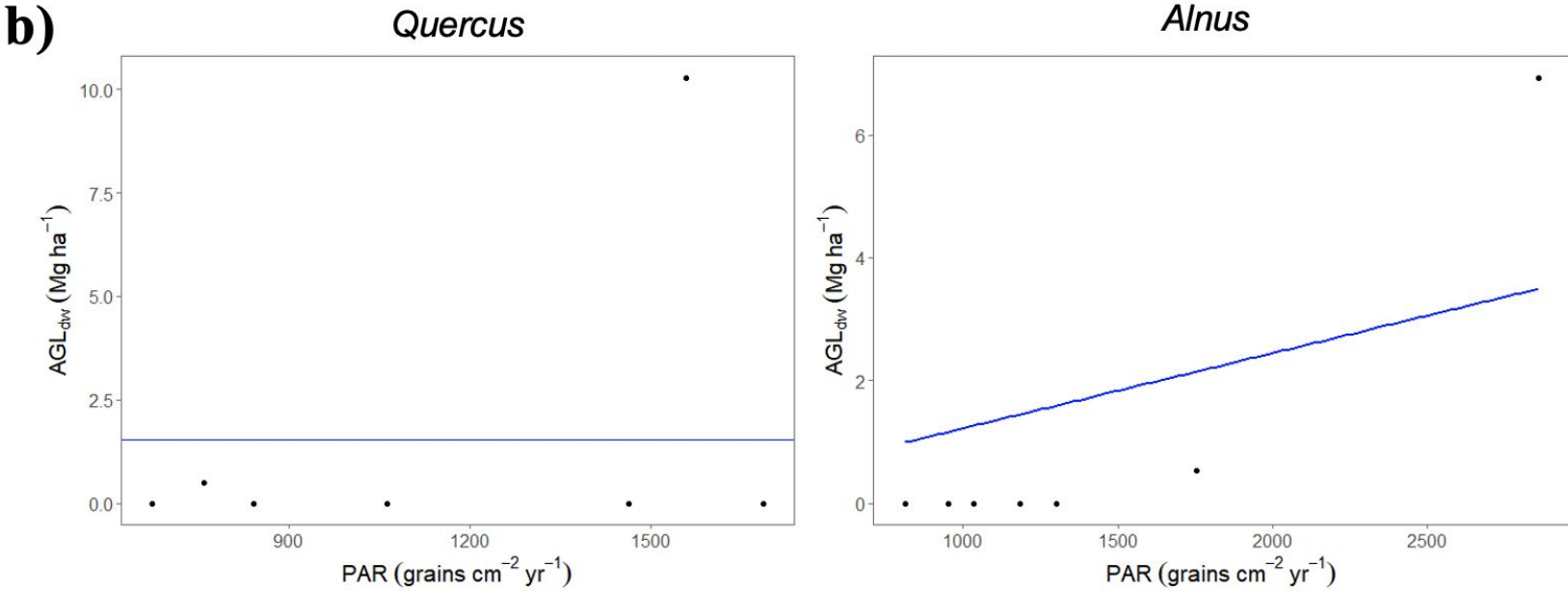


Figure 8b. The relationship between distance-weighted aboveground live biomass (AGL_{dw}) and pollen accumulation rate (PAR) for *Quercus* and *Alnus* at the seven lake sites in the Klamath Mountains. The line represents the intercept of the null model. The relevant source area of pollen was defined as a circle with a radius of 625 m from the centroid of the lake. For details on the linear model, see Table S11.

Table 1. Lake site characteristics and overstory vegetation at each site.

Lake site and code	Lat and long (dec. degrees)	Elevation (m)	Depth at deepest point/sample location (m)	Surface area (ha)	Mature overstory vegetation
Blue (BLU)	-123.69, 41.24	822	4.6	1.4	<i>C. lawsoniana</i> , <i>P. menziesii</i> , <i>C. chrysaphylla</i> , <i>N. densiflora</i> , <i>A. menziesii</i> , <i>A. rhombifolia</i> , <i>P. lambertiana</i> , <i>T. brevifolia</i>
Fish (FSH)	-123.68, 41.26	541	13	9.6	<i>C. lawsoniana</i> , <i>P. menziesii</i> , <i>P. lambertiana</i> , <i>N. densiflora</i> , <i>A. menziesii</i> , <i>A. rhombifolia</i> , <i>C. chrysaphylla</i>
North Twin (NTW)	-123.67, 41.32	1142	0.5	3.4	<i>P. menziesii</i> , <i>P. lambertiana</i> , <i>C. lawsoniana</i> , <i>C. chrysaphylla</i> , <i>P. jeffreyi</i> , <i>T. heterophylla</i> , <i>C. decurrens</i> , <i>N. densiflora</i> , <i>A. menziesii</i>
South Twin (STW)	-123.67, 41.31	1137	1.2	3.5	
Onion (ONO)	-123.75, 41.38	1356	1.5	0.66	<i>P. ponderosa</i> , <i>P. menziesii</i> , <i>A. magnifica</i> , <i>C. decurrens</i> , <i>A. concour</i> , <i>P. lambertiana</i> , <i>T. brevifolia</i>
Ogaromtoc (OGA)	-123.54, 41.49	600	6.3	1.74	<i>P. menziesii</i> , <i>N. densiflora</i> , <i>P. lambertiana</i> , <i>A. macrophylla</i> , <i>A. rhombifolia</i> , <i>A. menziesii</i> , <i>U. californica</i> , <i>C. decurrens</i> , <i>Q. kelloggii</i> , <i>Q. garryana</i>
Red Mountain (RED)	-123.69, 41.25	768	1.6	1.2	<i>C. lawsoniana</i> , <i>P. menziesii</i> , <i>P. lambertiana</i> , <i>N. densiflora</i> , <i>A. menziesii</i> , <i>A. rhombifolia</i> , <i>C. chrysaphylla</i>

Table 2. Definitions of RSAP, aRSAP, and tRSAP.

Term	Definitional basis and relevant literature
RSAP	Originally described by Sugita (1994) as the “smallest area within which reliable estimates of parameter values and asymptotic r^2 or likelihood function scores can be obtained.” The definition was refined as the “distance from a pollen deposition point beyond which the relationship between vegetation composition and pollen assemblage does not improve” (Bunting et al. 2004, with Sugita). Estimates are derived for the overall assemblage from extended R-value analysis (Parsons and Prentice 1981) through inspection of the likelihood function score plot. RSAP varies depending on which taxa and which sites are included in the analysis, thus is dependent on the assemblage chosen for analysis.
aRSAP	Identical to the standard RSAP, but with the addition of an “a” to denote that it is an assemblage-specific metric, in contrast to the tRSAP.
tRSAP	The RSAP concept can be extended to single taxa where pollen taxa are measured independently (e.g., PAR values rather than percentage values). In this situation, we define a taxon-specific Relevant Source Area of Pollen, the tRSAP, as the distance beyond which the correlation between PAR (Y) and distance-weighted plant abundance (ψ) summed to that distance for a single taxon does not improve (Jackson 1990).

Table 3. A comparison of observed to predicted distance-weighted aboveground live biomass (AGL_{dw}) for each lake site using the assemblage-level relevant source area pollen (aRSAP) estimates. Predicted AGL_{dw} is the mean from 10,000 resampling iterations; Standard Error is the standard deviation of the 10,000 samples; COV is the coefficient of variation (Standard Error/Predicted AGL_{dw}); Bias is the percent difference between predicted and observed AGL_{DW} .

Lake	Observed AGL_{dw} (Mg ha ⁻¹)	Predicted AGL_{dw} (Mg ha ⁻¹)	Standard Error (Mg ha ⁻¹)	COV (%)	Bias (%)
Blue	205	189	31.5	17	-7.8
Fish	197	195	31.8	16	-1.1
North Twin	242	251	32.0	13	3.7
Ogaromtoc	127	134	31.6	24	5.7
Onion	215	212	32.1	15	-1.1
Red Mountain	197	218	31.4	14	10.5
South Twin	180	217	31.6	15	20.5

Table 4. A comparison of observed to predicted distance-weighted aboveground live biomass (AGL_{dw}) for each lake site using taxon-specific source area pollen estimates (tRSAP). Predicted AGL_{dw} is the mean from 10,000 resampling iterations; Standard Error is the standard deviation of the 10,000 samples; COV is the coefficient of variation (Standard Error/Predicted AGL_{DW}); Bias is the percent difference between predicted and observed AGL_{dw} .

Lake	Observed AGL_{dw} (Mg ha ⁻¹)	Predicted AGL_{dw} (Mg ha ⁻¹)	Standard Error (Mg ha ⁻¹)	COV (%)	Bias (%)
Blue	196	189	31.5	17	-3.7
Fish	185	195	31.8	16	5.2
North Twin	239	251	32.0	13	4.9
Ogaromtoc	121	134	31.6	24	10.6
Onion	193	212	32.1	15	10.3
Red	184	218	31.4	14	18.4
South Twin	173	217	31.6	15	24.9

1
2
3
4
5
6
7
8
9
10
11
12
13
14
15
16
17
18
19
20
21
22
23
24
25
26
27
28
29
30
31
32
33
34
35
36
37
38
39
40
41
42
43
44
45
46
47
48
49
50
51
52
53
54
55
56
57
58
59
60

Supplemental Information

Title: Linking modern pollen accumulation rates to biomass: Quantitative vegetation reconstruction in the western Klamath Mountains

Authors: Clarke A. Knight, Mark Baskaran, M. Jane Bunting, Marie Champagne, Matthew D. Potts, David Wahl, James Wanket, John J. Battles

For Peer Review

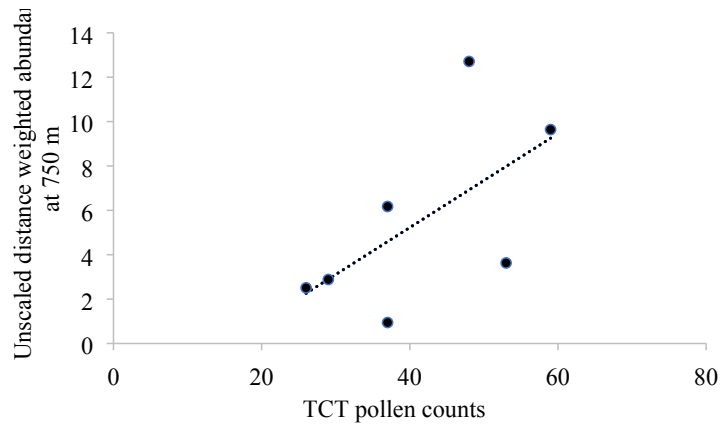


Figure S1. TCT pollen counts corrected to the same base sum plotted against unscaled distance weighted plant abundance at 750m to determine the reference taxon for the PolERV model.

Sediment dating and age-depth model

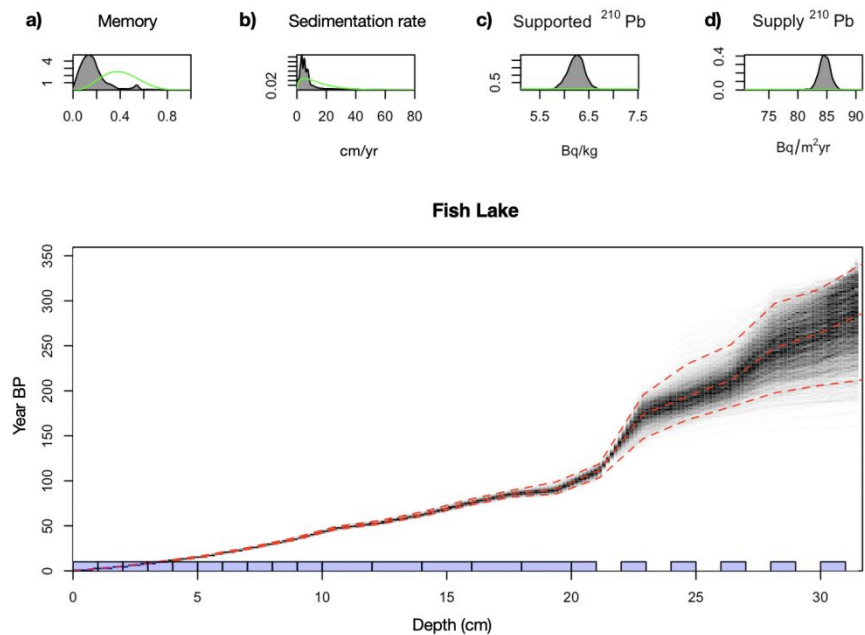
We used lead-210 (^{210}Pb ; 22.3 yr half-life) to assign ages to sediment deposited in the last 150 years. Surface bulk sediments from 0 cm to a maximum of 45 cm were taken from each core and dried to 105°C (see Tables S1-S7). ^{210}Pb activity was determined by alpha spectrometry, via ^{210}Po . An aliquot of 0.2 to 1.0 g of dried and pulverized sample was digested using concentrated HF, HNO₃, and HCl and a known amount of ^{209}Po spike in an oven at 90°C for ~ 24 hours. The digested solution was dried, and the residue was mixed with 1 M HCl until the pH was ~2. Auto-plating of Po was cold-plated onto an Ag disk for 24 hours at room temperature (Jweda and Baskaran 2011). The plated disk was assayed for Po using Octete PC ORTEC alpha spectrometer. The reagent blanks were run simultaneously with each batch of eight samples and were subtracted. Certified reference materials were periodically run. For the determination of parent-supported (i.e., background) ^{210}Pb , several samples were run for the activity of ^{226}Ra (using 352 and 609 keV) along with ^{137}Cs (661.6 keV) by Ge-well detector (Baskaran et al. 2015). Small sample sizes prevented reliable ^{137}Cs from being obtained.

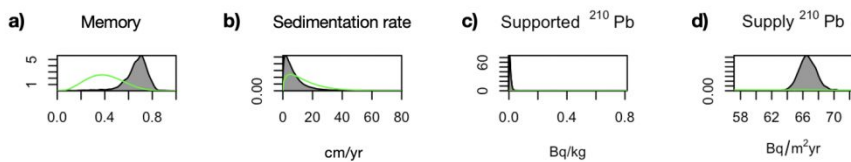
We used the Bayesian-based Plum software to develop age models from excess (unsupported) ^{210}Pb data (Aquino-López et al. 2018). The Plum model is related to the constant rate of supply (CRS) method (Appleby and Oldfield 1978) and retains two of the basic assumptions of CRS: the rate of supply of ^{210}Pb is constant and there is no vertical mixing of radionuclides. Testing these assumptions requires independent validation using another marker, which is outside of this paper's scope. The Plum model is formulated within a robust statistical framework to quantify uncertainty (Aquino-López et al. 2018). Plum uses a self-adjusting Markov Chain Monte Carlo (MCMC) algorithm called the t-walk (Christen and Fox 2010). Plum uses millions of MCMC iterations to model the accumulation of sediment, using a gamma

Commented [MOU1]: Moved from MS, as requested by Reviewer 2.

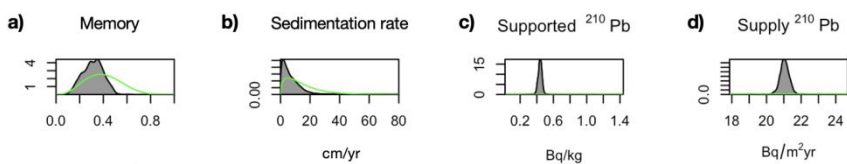
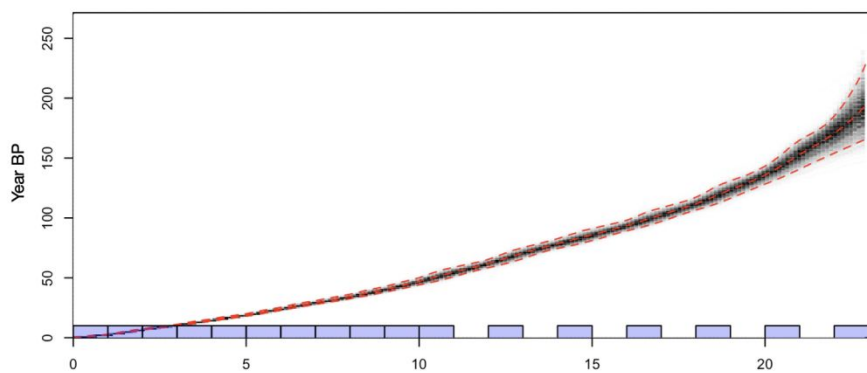
1
2
3
4
5
6
7
8
9
10 autoregressive semiparametric age-depth function (Blaauw and Christen 2011). This algorithm
11 results in a probability envelope around the mean age model. The envelope allows the precision
12 at any depth to be estimated explicitly. Plum makes use of prior information to determine the
13 datable horizon, which is affected by two factors: the precision of methodology (alpha versus
14 gamma counting) and the initial amount of excess lead. In Plum, the chronology limit is
15 determined by the rate of supply of ^{210}Pb to the site and the equipment error, usually ~ 3 Bq/kg
16 for a sample size of 1 g by alpha spectrometry for research laboratories. Supported ^{210}Pb
17 activities were determined from the direct measurements of ^{226}Ra by gamma-ray spectrometry.
18
19
20
21
22
23
24
25
26
27
28
29
30
31
32
33
34
35
36
37
38
39
40
41
42
43
44
45
46
47
48
49
50
51
52
53
54
55
56
57
58
59
60

Figure S2. The age-to-depth results of the Plum model for Fish, Ogaromtoc, Onion, North Twin, Red Mountain, and South Twin Lakes. The grey lines are simulation from Plum and the dashed red lines represent the mean age and the 95% interval. The small panels at the top show the prior (green) and posterior (grey) distributions for **(a)** the memory (ω), **(b)** the sedimentation rate (α), **(c)** the supported ^{210}Pb (P^S), which is the background level of ^{210}Pb already present in the sediment, and **(d)** the supply of ^{210}Pb (Φ).

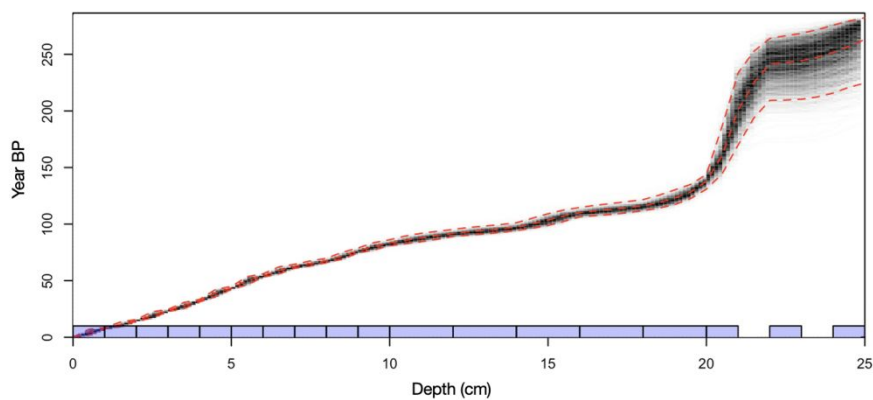


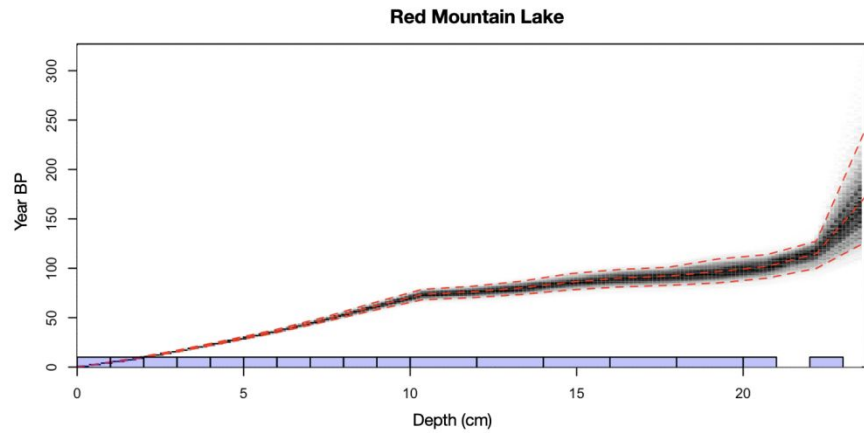
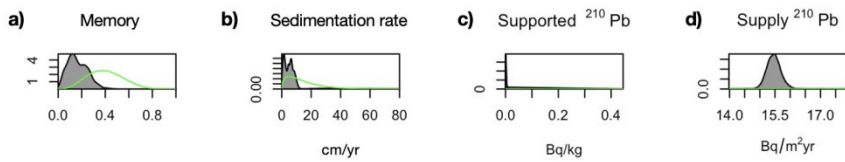
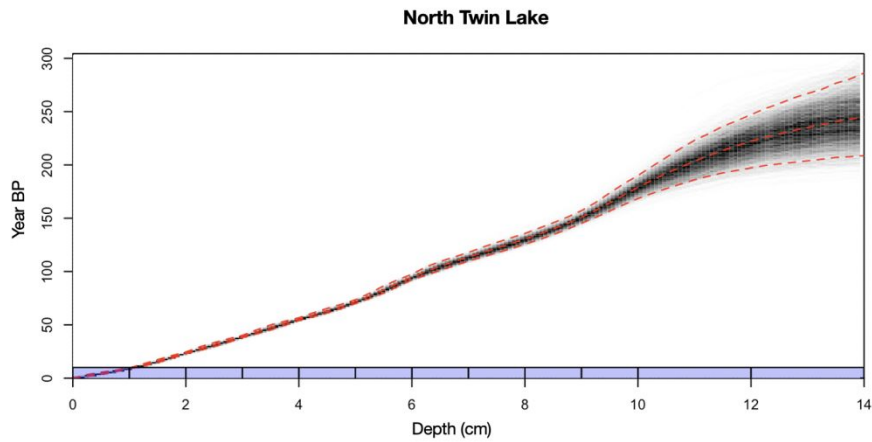
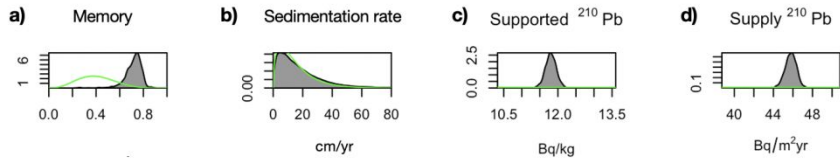


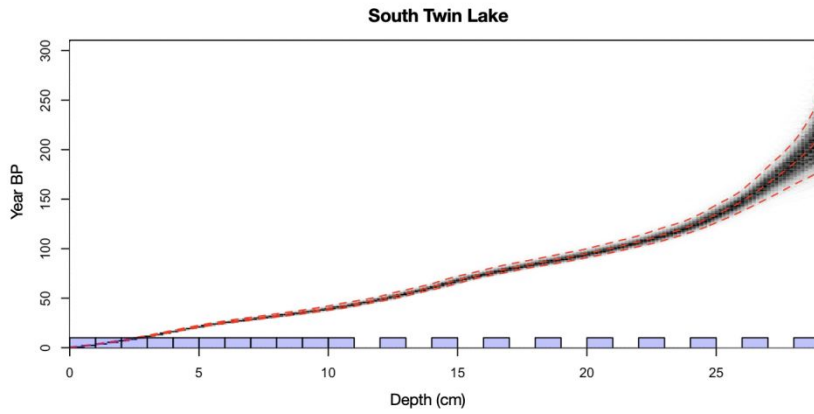
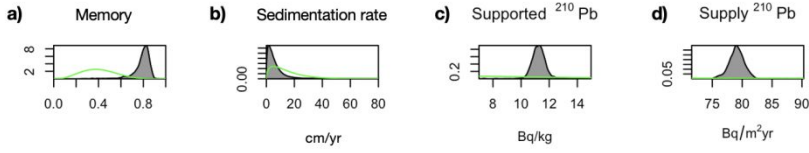
Ogaromtoc Lake



Onion Lake







Review

Lithology

Cores were split lengthwise and measured for magnetic susceptibility at every half centimeter using a calibrated MS2E surface scanning point sensor (MS Bartsoft). Changes in lithology were described and documented. The water content and dry bulk density were determined for each core in 1 or 2 cm intervals (Tables S14-S20), matching the sampling pattern for radioisotopic analysis (Table S1-S7).

Cores were composed of unlaminated gyttja. Occasional diatomaceous lenses (<1 cm thick) were present in Blue and Ogaromtoc lakes. For the Onion lake core, pine needles were visible in the top 3 cm, but needles were not seen in the other cores. Magnetic susceptibility was near zero for Blue, North Twin, Red Mountain, and South Twin lakes, and although magnetic susceptibility in Ogaromtoc lake was also generally low, Ogaromtoc had two distinct peaks (Fig. S3). Fish and Onion lakes showed higher overall magnetic susceptibility than the other lakes, as well as more variation across depths (Fig. S4). Peaks in magnetic susceptibility generally corresponded to increases in dry bulk density (g cm^{-3}) for Ogaromtoc, Fish, and Onion lakes (Tables S19, S17, S16, respectively). For example, two peaks at 14-15cm and 22-23cm in Ogaromtoc matched the depths where dry bulk density tripled and doubled, respectively. Ogaromtoc also had two light blue clay bands at 14-15cm and 22-23cm. Other cores did not contain clear stratigraphic markers.

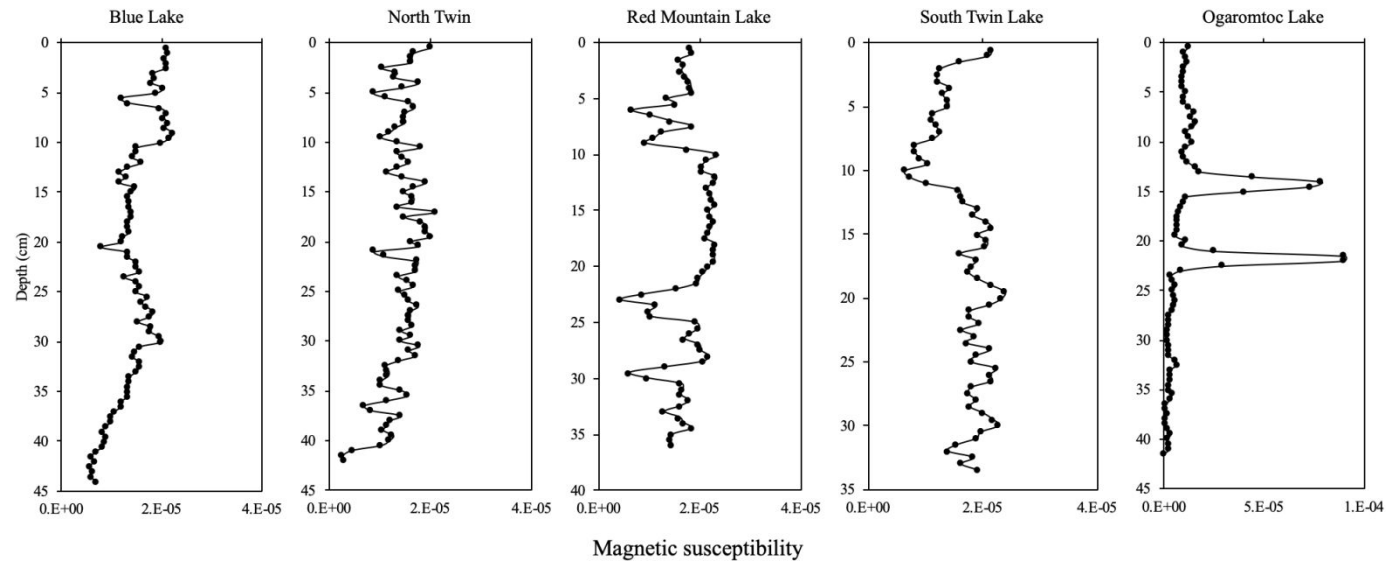


Figure S3. Magnetic susceptibility for the five study sites. The magnetic susceptibility was near zero with some variability for five lakes (note different x-axis for Ogaromtoc) – Blue, North Twin, Red Mountain, South Twin and Ogaromtoc Lakes.

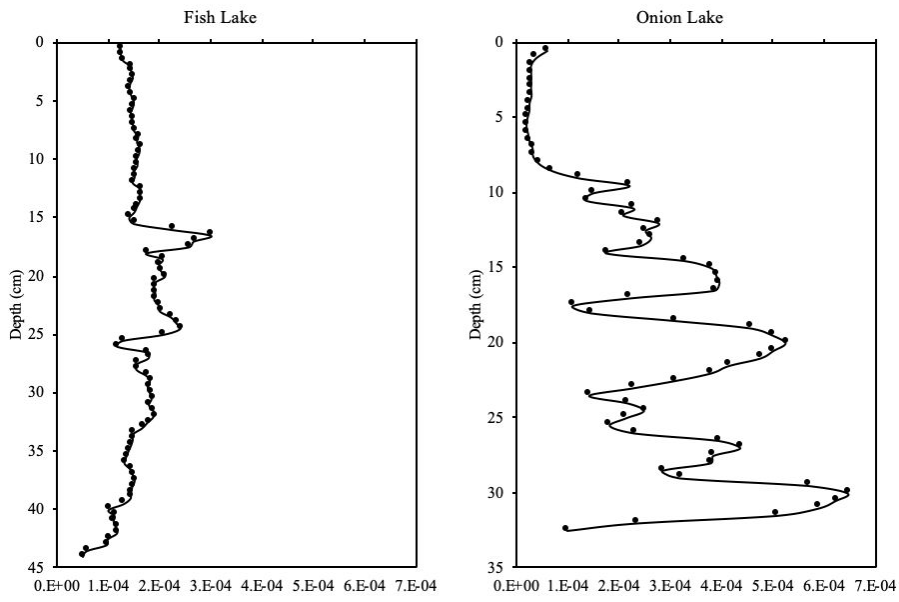


Figure S4. Magnetic susceptibility for the two study sites. Fish and Onion lakes (same x-axis) displayed higher overall magnetic susceptibility than the other five lake sites.

Table S1. ²¹⁰Pb dates used to create the Blue Lake age model.

Sample	Depth (cm)	Age (yr)	Uncertainty (yr)	Sample	Depth (cm)	Age (yr)	Uncertainty (yr)
210Pb_1	0.5	3	0.3	210Pb_12	13.0	38	2
210Pb_2	1.5	6	0.5	210Pb_13	15.0	45	3
210Pb_3	2.5	9	0.6	210Pb_14	17.0	50	3
210Pb_4	3.5	12	0.7	210Pb_15	19.0	57	4
210Pb_5	4.5	15	0.9	210Pb_16	20.5	69	5
210Pb_6	5.5	19	1	210Pb_17	22.5	87	9
210Pb_7	6.5	23	1	210Pb_18	24.5	103	13
210Pb_8	7.5	27	2	210Pb_19	26.5	125	21
210Pb_9	8.5	31	2	210Pb_20	28.5	146	27
210Pb_10	9.5	34	2	210Pb_21	30.5	175	57
210Pb_11	11.0	37	2				

Table S2. ²¹⁰Pb dates used to create the Fish Lake age model.

Sample	Depth (cm)	Age (yr)	Uncertainty (yr)	Sample	Depth (cm)	Age (yr)	Uncertainty (yr)
210Pb_1	0.5	2	0.2	210Pb_12	12.5	58	2
210Pb_2	1.5	5	0.4	210Pb_13	14.5	70	3
210Pb_3	2.5	8	0.5	210Pb_14	16.5	82	4
210Pb_4	3.5	12	0.6	210Pb_15	18.5	90	6
210Pb_5	4.5	15	0.7	210Pb_16	20.5	110	7
210Pb_6	5.5	20	0.8	210Pb_17	22.5	175	25
210Pb_7	6.5	25	1	210Pb_18	24.5	197	32
210Pb_8	7.5	30	1	210Pb_19	26.5	224	40
210Pb_9	8.5	36	1	210Pb_20	28.5	244	51
210Pb_10	9.5	44	2	210Pb_21	30.5	277	60
210Pb_11	10.5	49	2				

1:

Table S3. ^{210}Pb dates used to create the Ogaromtoc Lake age model. An outlier point at 6.5cm was excluded from the model.

Sample	Depth (cm)	Age (yr)	Uncertainty (yr)	Sample	Depth (cm)	Age (yr)	Uncertainty (yr)
210Pb_1	0.5	3	0.2	210Pb_9	9.5	47	3
210Pb_2	1.5	7	0.4	210Pb_10	10.5	55	4
210Pb_3	2.5	11	0.6	210Pb_11	12.5	71	5
210Pb_4	3.5	15	0.8	210Pb_12	14.5	86	5
210Pb_5	4.5	19	1	210Pb_13	16.5	103	6
210Pb_6	5.5	24	1	210Pb_14	18.5	124	7
210Pb_7	7.5	34	2	210Pb_15	20.5	153	12
210Pb_8	8.5	40	2	210Pb_16	22.5	197	34

Table S4. ^{210}Pb dates used to create the Onion Lake age model.

Sample	Depth (cm)	Age (yr)	Uncertainty (yr)	Sample	Depth (cm)	Age (yr)	Uncertainty (yr)
210Pb_1	0.5	8	0.6	210Pb_10	9.5	83	3
210Pb_2	1.5	15	0.7	210Pb_11	11.0	88	4
210Pb_3	2.5	24	0.9	210Pb_12	13.0	94	4
210Pb_4	3.5	32	1	210Pb_13	15.0	104	5
210Pb_5	4.5	44	1	210Pb_14	17.0	113	5
210Pb_6	5.5	54	2	210Pb_15	19.0	123	7
210Pb_7	6.5	63	2	210Pb_16	20.5	201	32
210Pb_8	7.5	68	2	210Pb_17	22.5	244	29
210Pb_9	8.5	77	2	210Pb_18	24.5	263	29

Table S5. ^{210}Pb dates used to create the North Twin Lake age model.

Sample	Depth (cm)	Age (yr)	Uncertainty (yr)	Sample	Depth (cm)	Age (yr)	Uncertainty (yr)
210Pb_1	0.5	2	0.4	210Pb_7	6.5	112	4
210Pb_2	1.5	24	0.8	210Pb_8	7.5	128	5
210Pb_3	2.5	39	1	210Pb_9	8.5	147	6
210Pb_4	3.5	55	1	210Pb_10	9.5	173	10
210Pb_5	4.5	71	2	210Pb_11	11.0	197	18
210Pb_6	5.5	94	3	210Pb_12	13.0	229	30

1.

Table S6. ²¹⁰Pb dates used to create the Red Mountain Lake age model.

Sample	Depth (cm)	Age (yr)	Uncertainty (yr)	Sample	Depth (cm)	Age (yr)	Uncertainty (yr)
210Pb_1	0.5	5	0.3	210Pb_10	9.5	71	5
210Pb_2	1.5	10	0.2	210Pb_11	11.0	75	6
210Pb_3	2.5	16	0.8	210Pb_12	13.0	79	7
210Pb_4	3.5	23	1	210Pb_13	15.0	87	8
210Pb_5	4.5	30	2	210Pb_14	17.0	91	9
210Pb_6	5.5	37	2	210Pb_15	19.0	96	12
210Pb_7	6.5	45	2	210Pb_16	20.5	104	12
210Pb_8	7.5	53	3	210Pb_17	22.5	146	37
210Pb_9	8.5	62	4				

Table S7. ²¹⁰Pb dates used to create the South Twin Lake age model.

Sample	Depth (cm)	Age (yr)	Uncertainty (yr)	Sample	Depth (cm)	Age (yr)	Uncertainty (yr)
210Pb_1	0.5	3	0.3	210Pb_11	10.5	44	3
210Pb_2	1.5	7	0.4	210Pb_12	12.5	55	3
210Pb_3	2.5	12	0.6	210Pb_13	14.5	68	4
210Pb_4	3.5	17	0.8	210Pb_14	16.5	80	4
210Pb_5	4.5	22	1	210Pb_15	18.5	90	4
210Pb_6	5.5	26	1	210Pb_16	20.5	95	5
210Pb_7	6.5	29	1	210Pb_17	22.5	114	7
210Pb_8	7.5	33	2	210Pb_18	24.5	135	9
210Pb_9	8.5	36	2	210Pb_19	26.5	166	16
210Pb_10	9.5	40	2	210Pb_20	28.5	186	38

Assumptions of the Prentice-Sugita-Sutton PVM

Commented [MOU2]: Added for Reviewer 3

As noted in section 2.2, the Prentice-Sugita-Sutton model has certain assumptions (Sugita 1994, Gaillard et al. 2008), which we describe in full here:

- 1) that there is a comprehensible and spatially and temporally consistent relationship between pollen loading and distance-weighted plant abundance
- 2) the vegetation surface where the pollen is derived from is flat
- 3) the sampling basin is a circular opening in the canopy
- 4) pollen productivity (the amount of pollen produced per vegetation cover unit) is a constant for a given pollen taxon
- 5) pollen is dispersed as single grains
- 6) pollen dispersal is largely via wind above the canopy and gravity beneath the canopy, and pollen transport into a basin (canopy opening) can be modelled by considering the canopy component only
- 7) wind is uniform in every direction therefore pollen dispersal is evenly distributed around the source
- 8) most pollen deposition takes place via sedimentation due to gravity and deposition by interception is negligible
- 9) the deposition of pollen at a specified distance from a plant can be approximated using a diffusion model of the dispersal of small particles from a ground level source (Sutton 1953)
- 10) inter-taxon pollen grain differences (e.g., grain size, weight, and density) affect pollen dispersal and can be quantitatively estimated, and use of a single value to represent each taxon is sufficient to capture

- 1
2
3
4
5
6
7
8
9
10 11) atmospheric conditions during pollen deposition can be modelled as “stable” which
11 affects parameters C_z and n (Eq.3,3a)
12
13 12) all lake sites experience the same conditions
14
15
16
17

18 *PAR calculation*

19
20 After grains were counted, pollen concentrations and PAR were determined. Using the
21 *Lycopodium* marker grains, pollen concentrations (C_i , grains cm^{-3}) were calculated for each
22 pollen type i using the following equation:
23
24

$$25 \quad C_i = \frac{A_i \times L_a}{L_c \times V_i} \quad (6)$$

26
27 Where A_i is the number of pollen grains counted for the taxon i , L_a is the number of added
28 marker grains, L_c is the number of counted marker grains in each slide, and V_i is the volume of
29 the pollen sample (e.g., 0.63 cm^3) (Stockmarr 1971). Concentrations were used for PAR
30 calculations by multiplying the concentration values by the sediment accumulate rate, which
31 differed by lake site and was determined by the Plum age model in increments of 0.5cm. The
32 equation used was:
33
34
35
36

$$37 \quad PAR_i = C_i \times S \quad (7)$$

38
39 Where PAR_i is the pollen accumulation rate for taxon i , C_i is the pollen concentration (grains cm^{-3})
40 for taxon i , and S is the sedimentation rate (cm yr^{-1}) (Davis and Deevey 1964).
41
42
43
44
45
46
47
48
49
50
51
52
53
54
55
56
57
58
59
60

Commented [MOU3]: Moved these equations, as requested by Reviewer 2.

Table S8. Coefficients for the predicted aboveground live biomass (Mg ha^{-1}) of trees as a function of basal area ($\text{m}^2 \text{ha}^{-1}$) using a linear log-log (natural) equation. Results for all species encountered in the forest inventory conducted for the seven lakes in the Klamath Mountains. The p-value of the regression was < 0.0001 in all cases except for white alder where $p = 0.034$. B_0 is the intercept; B_1 is the slope coefficient; SEE = standard error of the estimate.

Genus	Species	Common name	B_0	B_1	R^2_{adj}	SEE (Mg ha^{-1})
<i>Abies</i>	<i>concolor</i>	white fir	1.65	1.07	0.95	0.40
<i>Abies</i>	<i>magnifica</i>	California red fir	1.47	1.19	0.92	0.46
<i>Acer</i>	<i>macrophyllum</i>	bignleaf maple	1.30	1.11	0.94	0.24
<i>Alnus</i>	<i>rhombifolia</i>	white alder	1.26	1.30	1.00	0.07
<i>Arbutus</i>	<i>menziesii</i>	Pacific madrone	1.55	1.12	0.94	0.29
<i>Calocedrus</i>	<i>decurrens</i>	incense-cedar	1.08	1.18	0.90	0.52
<i>Chamaecyparis</i>	<i>lawsoniana</i>	Port-Orford-cedar	1.16	1.19	0.97	0.37
<i>Chrysolepis</i>	<i>chrysophylla</i>	golden chinquapin	1.19	1.18	0.96	0.34
<i>Cornus</i>	<i>nuttallii</i>	Pacific dogwood	1.07	0.92	0.85	0.37
<i>Notholithocarpus</i>	<i>densiflorus</i>	tanoak	1.08	1.17	0.96	0.35
<i>Pinus</i>	<i>attenuata</i>	knobcone pine	1.18	1.06	0.96	0.21
<i>Pinus</i>	<i>jeffreyi</i>	Jeffrey pine	1.09	1.11	0.88	0.58
<i>Pinus</i>	<i>lambertiana</i>	sugar pine	1.67	1.22	0.85	0.59
<i>Pinus</i>	<i>ponderosa</i>	ponderosa pine	1.36	1.23	0.89	0.50
<i>Pseudotsuga</i>	<i>menziesii</i>	Douglas-fir	1.15	1.23	0.96	0.30
<i>Quercus</i>	<i>chrysolepis</i>	canyon live oak	1.47	1.12	0.92	0.43
<i>Quercus</i>	<i>kelloggii</i>	California black oak	1.62	1.11	0.96	0.27
<i>Taxus</i>	<i>brevifolia</i>	Pacific yew	0.83	0.82	0.94	0.21
<i>Umbellularia</i>	<i>californica</i>	California-laurel	0.95	1.30	0.95	0.38

Table S9. Fall speed (m/sec) for major taxa used in the simulation runs of this study.

Taxa	Fall-speed (v_s) estimates ($m\ s^{-1}$)
<i>Abies</i>	0.120 ^a
<i>Alnus</i>	0.021 ^b
<i>Pinus</i>	0.031 ^a
<i>Pseudotsuga</i>	0.126 ^a
<i>Quercus</i>	0.035 ^a
<i>TCT</i>	0.016 ^c

^a Eisenhut (1961); ^b Schober (1975);

^c Calculated from empirical measurements using Stoke's Law with Falck's (1927) correction

Table S10. PAR values of main taxa from 2018 (a modeled age) at each lake site.

Lake Site	<i>Pinus</i>	<i>Pseudotsuga</i>	<i>Quercus</i>	<i>TCT</i>	<i>Notholithocarpus</i>	<i>Alnus</i>	<i>Abies</i>
Blue	1760	5461	758	4490	1031	1183	789
Red Mt.	3672	5068	672	3051	2844	1034	569
Onion	10797	2014	1063	1622	559	951	4811
North Twin	1749	6808	1686	2311	2935	812	1999
South Twin	2384	7152	1463	2005	2059	1300	325
Fish	1479	4606	840	1782	3741	2858	34
Ogaromtoc	3376	4609	1558	844	454	1753	260

Table S11. Results from the linear regressions predicting distance-weighted aboveground live biomass (AGL_{dw}) as a function of pollen accumulation rate (PAR) for the pollen taxa present at the seven lake sites in the Klamath Mountains. The assemblage-level relevant source area of pollen (aRSAP) was defined as a circle with a radius of 625 m from centroid of the lake. Parameters provided the linear regression: $AGL_{DW} = B_0 + B_1 * PAR$ where AGL_{dw} is measured in $Mg\ ha^{-1}$; PAR in $grains\ cm^{-2}\ yr^{-1}$; SEE = standard error of the estimate; $\Delta AICc$ = the difference in the Akaike Information Criterion for small samples between the top ranked model and the second ranked model.

Commented [MOU4]: Added AICc for Reviewer 3.

Pollen Taxa	$\Delta AICc$	B_0	B_1	SEE ($Mg\ ha^{-1}$)	R^2_{adj}	P
<i>Pseudotsuga</i>	6.6	0	0.0180	19.1	0.96	< 0.001
<i>Pinus</i>	5.4	0	0.00740	8.42	0.94	<0.001
<i>Notholithocarpus</i>	4.2	0	0.0211	16.5	0.89	<0.001
TCT	4.0	0	0.00954	9.43	0.87	<0.001
<i>Quercus</i> ¹	--	--	--	--	--	--
<i>Alnus</i>	3.0	3.8	0.00341	1.05	0.84	0.002
<i>Abies</i>	4.2	0	0.0138	13.8	0.80	0.0018

¹There was no evidence of a significant linear relationship for *Quercus*. For predicting AGL_{dw} , a null model was used with the intercept = 1.54 and the standard error = 1.46.

Table S12. Results from the linear regressions predicting distance-weighted aboveground live biomass (AGL_{dw}) as a function of pollen accumulation rate (PAR) for the pollen taxa present at the seven lake sites in the Klamath Mountains. The taxon-specific source area of pollen (tRSAP) was defined as a circle with a radius determined by the strength of correlation (R^2) between plant abundance and PAR. Parameters provided the linear regression: $AGL_{dw} = B_0 + B_1 * PAR$ where AGL_{DW} is measured in $Mg\ ha^{-1}$; PAR in $grains\ cm^{-2}\ yr^{-1}$; SEE = standard error of the estimate.

Pollen Taxa	B_0	B_1	SEE ($Mg\ ha^{-1}$)	R^2_{adj}	P
<i>Pseudotsuga</i>	0	0.0180	19.1	0.96	< 0.001
<i>Pinus</i>	0	0.00558	6.78	0.95	<0.001
<i>Notholithocarpus</i>	0	0.0205	16.2	0.91	<0.001
TCT	0	0.00849	8.97	0.87	<0.001
<i>Quercus</i> ¹	--	--	--	--	--
<i>Alnus</i>	-3.8	0.00341	1.05	0.84	0.002
<i>Abies</i>	0	0.0138	13.8	0.83	0.0018

¹There was no evidence of a significant linear relationship for *Quercus*. For predicting AGL_{dw} , a null model was used with the intercept = 1.54 and the standard error = 1.46.

Table S13. Results from the linear regressions predicting distance-weighted aboveground live biomass (AGL_{dw}) as a function of pollen accumulation rate (PAR) for the pollen taxa present at the seven lake sites in the Klamath Mountains. These equations all include an intercept and slope term even if they were not the best fit. The relevant source area of pollen (aRSAP) was defined as a circle with a radius of 625 m from centroid of the lake. Parameters provided the linear regression: $AGL_{DW} = B_0 + B_1 * PAR$ where AGL_{dw} is measured in $Mg\ ha^{-1}$; PAR in $grains\ cm^{-2}\ yr^{-1}$; SEE = standard error of the estimate.

Pollen Taxa	B_0	B_1	SEE ($Mg\ ha^{-1}$)	R^2_{adj}	P
<i>Pseudotsuga</i>	-14.7	0.0206	20.3	0.74	0.008
<i>Pinus</i>	-5.5	0.00829	8.23	0.92	<0.001
<i>Notholithocarpus</i>	16.8	0.0149	14.7	0.61	0.02
TCT	-12.1	0.0138	8.33	0.78	0.005
<i>Quercus</i>	-2.9	0.00386	3.84	0.0083	0.4
<i>Alnus</i>	-3.8	0.00341	1.05	0.84	0.002
<i>Abies</i>	-9.4	0.0168	12.35	0.84	0.002

Table S14. Dry bulk density (g cm^{-3}) for Blue Lake.

Lake	Depth (cm)	Dry Bulk Density (g cm^{-3})
Blue	0-1	0.102
Blue	1-2	0.093
Blue	2-3	0.085
Blue	3-4	0.095
Blue	4-5	0.088
Blue	5-6	0.087
Blue	6-7	0.089
Blue	7-8	0.085
Blue	8-9	0.084
Blue	9-10	0.078
Blue	10-12	0.087
Blue	12-14	0.096
Blue	14-16	0.102
Blue	16-18	0.093
Blue	18-20	0.095
Blue	20-21	0.095
Blue	22-23	0.104
Blue	24-25	0.089
Blue	26-27	0.090
Blue	28-29	0.090
Blue	30-31	0.093
Blue	40-42	0.124

Table S15. Dry bulk density (g cm^{-3}) for Red Mountain Lake.

Lake	Depth (cm)	Dry Bulk Density (g cm^{-3})
Red Mt.	0-1	0.080
Red Mt.	1-2	0.090
Red Mt.	2-3	0.074
Red Mt.	3-4	0.078
Red Mt.	4-5	0.068
Red Mt.	5-6	0.068
Red Mt.	6-7	0.071
Red Mt.	7-8	0.074
Red Mt.	8-9	0.079
Red Mt.	9-10	0.074
Red Mt.	10-12	0.081
Red Mt.	12-14	0.090
Red Mt.	14-16	0.112
Red Mt.	16-18	0.098
Red Mt.	18-20	0.110
Red Mt.	20-21	0.100
Red Mt.	22-23	0.121
Red Mt.	24-25	0.141
Red Mt.	26-27	0.146
Red Mt.	28-29	0.144
Red Mt.	30-31	0.150
Red Mt.	35-37	0.158

Table S16. Dry bulk density (g cm^{-3}) for Onion Lake.

Lake	Depth (cm)	Dry Bulk Density (g cm^{-3})
Onion	0-1	0.084
Onion	1-2	0.093
Onion	2-3	0.082
Onion	3-4	0.074
Onion	4-5	0.073
Onion	5-6	0.065
Onion	6-7	0.049
Onion	7-8	0.047
Onion	8-9	0.061
Onion	9-10	0.082
Onion	10-12	0.128
Onion	12-14	0.140
Onion	14-16	0.157
Onion	16-18	0.195
Onion	18-20	0.224
Onion	20-21	0.235
Onion	22-23	0.227
Onion	24-25	0.228
Onion	26-27	0.246
Onion	28-29	0.189
Onion	30-31	0.223

Table S17. Dry bulk density (g cm^{-3}) for Fish Lake.

Lake	Depth (cm)	Dry Bulk Density (g cm^{-3})
Fish	0-1	0.101
Fish	1-2	0.099
Fish	2-3	0.101
Fish	3-4	0.100
Fish	4-5	0.101
Fish	5-6	0.100
Fish	6-7	0.107
Fish	7-8	0.101
Fish	8-9	0.115
Fish	9-10	0.120
Fish	10-11	0.117
Fish	12-13	0.142
Fish	14-15	0.149
Fish	16-17	0.541
Fish	18-19	0.198
Fish	20-21	0.222
Fish	22-23	0.286
Fish	24-25	0.494
Fish	26-27	0.198
Fish	28-29	0.187
Fish	30-31	0.203

Table S18. Dry bulk density (g cm^{-3}) for South Twin Lake.

Lake	Depth (cm)	Dry Bulk Density (g cm^{-3})
South Twin	0-1	0.076
South Twin	1-2	0.073
South Twin	2-3	0.067
South Twin	3-4	0.059
South Twin	4-5	0.054
South Twin	5-6	0.050
South Twin	6-7	0.045
South Twin	7-8	0.047
South Twin	8-9	0.047
South Twin	9-10	0.050
South Twin	10-11	0.051
South Twin	12-13	0.060
South Twin	14-15	0.064
South Twin	16-17	0.073
South Twin	18-19	0.067
South Twin	20-21	0.075
South Twin	22-23	0.083
South Twin	24-25	0.110
South Twin	26-27	0.130
South Twin	28-29	0.130
South Twin	30-31	0.154

Table S19. Dry bulk density (g cm^{-3}) for Ogaromtoc Lake.

Lake	Depth (cm)	Dry Bulk Density (g cm^{-3})
Ogaromtoc	0-1	0.086
Ogaromtoc	1-2	0.083
Ogaromtoc	2-3	0.064
Ogaromtoc	3-4	0.064
Ogaromtoc	4-5	0.065
Ogaromtoc	5-6	0.068
Ogaromtoc	6-7	0.072
Ogaromtoc	7-8	0.074
Ogaromtoc	8-9	0.071
Ogaromtoc	9-10	0.066
Ogaromtoc	10-11	0.068
Ogaromtoc	12-13	0.081
Ogaromtoc	14-15	0.366
Ogaromtoc	16-17	0.116
Ogaromtoc	18-19	0.072
Ogaromtoc	20-21	0.096
Ogaromtoc	22-23	0.268
Ogaromtoc	24-25	0.147
Ogaromtoc	26-27	0.066
Ogaromtoc	28-29	0.061
Ogaromtoc	30-31	0.064

Table S20. Dry bulk density (g cm^{-3}) for North Twin Lake.

Lake	Depth (cm)	Dry Bulk Density (g/cm^3)
North Twin	0-1	0.099
North Twin	1-2	0.097
North Twin	2-3	0.101
North Twin	3-4	0.107
North Twin	4-5	0.108
North Twin	5-6	0.106
North Twin	6-7	0.092
North Twin	7-8	0.076
North Twin	8-9	0.076
North Twin	9-10	0.088
North Twin	10-12	0.132
North Twin	12-14	0.143
North Twin	14-16	0.145
North Twin	16-18	0.145
North Twin	18-20	0.141
North Twin	20-21	0.122
North Twin	22-23	0.133
North Twin	24-25	0.127
North Twin	26-27	0.137
North Twin	28-29	0.135
North Twin	30-31	0.137

References

- Appleby P and Oldfield F (1978) The calculation of lead-210 dates assuming a constant rate of supply of unsupported ^{210}Pb to the sediment. *Catena* 5:1–8.
- Baskaran M, Miller CJ, Kumar A et al. (2015) Sediment accumulation rates and sediment dynamics using five different methods in a well-constrained impoundment: Case study from Union Lake, Michigan. *Journal of Great Lakes Research* 41:607–617.
- Davis MB and Deevey ES (1964) Pollen accumulation rates: estimates from Late-Glacial sediment Rogers Lake. *Science* 145:1293–1295.
- Eisenhut G (1961) Untersuchungen über die Morphologie und Ökologie der Pollenkörner heimischer und fremdländischer Waldbäume. Paul Parey, Hamburg.
- Falck R (1927) Über die Größen, Fallgeschwindigkeit und Schwebewerte der Pilzsporen und ihre Gruppierung mit Bezug auf die zu ihre Verbreitung nötigen temperaturströmungs-Geschwindigkeit. *Berichte der Deutschen Botanischen Gesellschaft* 45:262–281.
- Gaillard MJ, Sugita S, Bunting MJ et al. (2008) The use of modelling and simulation approach in reconstructing past landscapes from fossil pollen data: a review and results from the POLLANDCAL network. *Vegetation History and Archaeobotany* 17:419–443.
- Jweda J and Baskaran M (2011) Interconnected riverine-lacustrine systems as sedimentary repositories: Case study in southeast Michigan using ^{210}Pb and ^{137}Cs sediment accumulation and mixing models. *Journal of Great Lakes Research* 37:432–446.
- Schober, R., 1975. Ertragstabellen wichtiger Baumarten bei verschiedener Durchforstung. Sauerländer, Frankfurt a. M.
- Stockmarr J (1971) Tablets with spores used in pollen analysis. *Pollen and Spores* 13:615–621.
- Sugita S (1994) Pollen representation of vegetation in Quaternary sediments: Theory and method in patchy vegetation. *Journal of Ecology* 82:881–897.